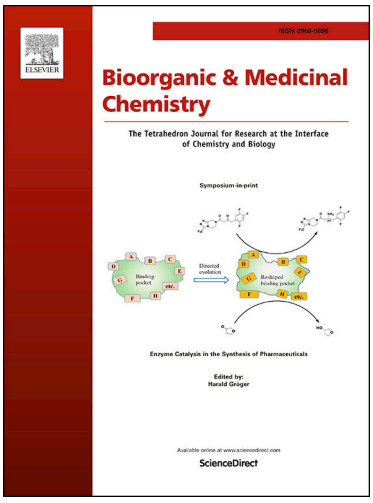

Rational design, synthesis and biological profiling of new KDM4C inhibitors

Vatroslav Letfus, Dubravko Jelić, Ana Bokulić, Adriana Petrinić Grba, Sanja Koštrun

PII: S0968-0896(19)31071-5
DOI: https://doi.org/10.1016/j.bmc.2019.115128
Reference: BMC 115128

To appear in: *Bioorganic & Medicinal Chemistry*

Received Date: 26 June 2019
Revised Date: 12 September 2019
Accepted Date: 18 September 2019

Please cite this article as: V. Letfus, D. Jelić, A. Bokulić, A. Petrinić Grba, S. Koštrun, Rational design, synthesis and biological profiling of new KDM4C inhibitors, *Bioorganic & Medicinal Chemistry* (2019), doi: https://doi.org/10.1016/j.bmc.2019.115128

Graphical Abstract

Rational design, synthesis and biological profiling of new KDM4C inhibitors

Leave this area blank for abstract info.

Vatroslav Letfus*, Dubravko Jelić, Ana Bokulić, Adriana Petrinić Grba, Sanja Koštrun
Fidelta Ltd., Prilaz baruna Filipovića 29, 10000 Zagreb, Croatia

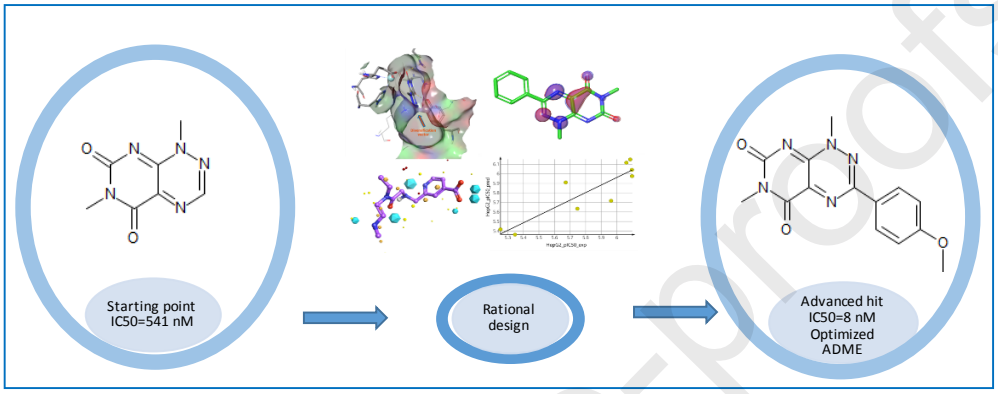

ELSEVIER

Bioorganic & Medicinal Chemistry
journal homepage: www.elsevier.com

Rational design, synthesis and biological profiling of new KDM4C inhibitors

Vatroslav Letfus*, Dubravko Jelić, Ana Bokulić, Adriana Petrinić Grba, Sanja Koštrun
Fidelta Ltd., Prilaz baruna Filipovića 29,10000 Zagreb, Croatia

ARTICLE INFO

Article history:
Received
Received in revised form
Accepted
Available online

Keywords:
Epigenetics
KDM4C enzyme
Inhibitor
Drug design
Computational chemistry

ABSTRACT

The human histone demethylases of the KDM4 family have been related to diseases such as prostate and breast cancer. Majority of currently known inhibitors suffer from the low permeability and low selectivity between the enzyme isoforms. In this study, toxoflavin motif was used to design and synthesize new KDM4C inhibitors with improved biological activity and *in vitro* ADME properties. Inhibitors displayed good passive cellular permeability and metabolic stability. However, diminishing of redox liability and consequently non-specific influence on cell viability still remains a challenge.

1. Introduction

Chromatin is a complex aggregation of DNA and histone proteins that allows large amounts of DNA to fit in the restricted space of a eukaryotic cell's nucleus.[1] Dynamic regulation of its structure is needed to maintain the processes that require access to DNA in response to physiological and environmental changes.[2]

Methylation of lysine amino acid residues on histones plays a significant role in the epigenetic regulation of gene expression by applying different transcription factors to the chromatin.[3-5] Homeostasis of these methylation motifs by different histone lysine methyl transferase and histone lysine demethylase enzymes (KDMs) is of key importance to preserve proper cellular development and to enable differentiation of cells.[6-7] Dysregulation of histone lysine methylations has been linked to deviant gene expression and malignant transformations.[8-10]

Histone lysine methylation is a reversible process. The removal of methyl groups is catalyzed by two enzyme families. The first is flavin-dependent lysine specific demethylase (LSD/KDM1) family that demethylate mono- and dimethyl lysine substrates. The second family is comprised of several enzymes, which are members of the Jumonji C (JmjC) domain containing Fe^{2+} and α-ketoglutarate dependent di-oxygenase enzymes which can additionally convert trimethyl lysine substrates to their dimethyl forms. These enzymes are further classified into seven sub-families (KDM2-8) based on their sequence similarities and domain architectures.

The KDM4 sub-family consists of five enzymes, KDM4A, KDM4B, KDM4C, KDM4D and KDM4E. They share extensive homology at their N-terminal part harboring the catalytic domain. KDM4A-C share more than 50% sequence identity and their protein structures includes a JMJN and JMJC domains, two PHD and two Tudor domains.

KDM4A, B and C are capable of catalyzing demethylation of lysine residues 9 (H3K9) and 36 (H3K36) on histone 3, while KDM4D is selective for the demethylation of only H3K9. Moreover, KDM4A and KDM4C, compared to KDM4B, seem to be much more catalytically active. Thus, the five KDM4 family members exhibit different biochemistry and are thought to perform distinct physiological functions.[11-12]

Over-expressions of KDMs are implicated in various diseases [12-16] and are considered to promote oncogenesis in several cancer types, mainly prostate, breast and colon.[16,17] Furthermore, results from Garcia *et al*. suggest that the histone demethylase activity of KDM4C enzyme is essential for breast cancer progression given its role in the maintenance of chromosomal stability and cell growth, thus emphasizing it as a promising therapeutic target.[18]

So far, only a few KDM inhibitors are reported, most of which function via active site metal chelation.[15] The majority of known inhibitors are analogues of the 2-oxoglutarate co-factor (2-OG), such as N-oxalyl glycine, 2,4-pyridine dicarboxylic acid, or consist of strong metal chelators, such as 2,2-bipyridines or hydroxyquinolines.[19] Although these compounds may be potent biochemical inhibitors, their physicochemical properties limit ADME properties, especially cell permeability. Two papers from GSK reported inhibitors with enhanced properties and cell permeability, but these compounds still have significant activity against related histone demethylases.[20-21] The combination of moderate biochemical activity and limited cell permeability leaves space for further investigation and design of novel compounds as chemical tools or potential drug candidates.

Tox
KDM4C[23] inhibitor (IC_{50}= 0.5 μM). Five-fold increase in activity is observed for KDM4C, which makes the toxoflavin a good initial hit for the design of KDM4C inhibitors. Anticancer activity was observed in both liquid and solid tumor cells, with a dose- and time-dependent effect.[22] However, a strong redox liability (poisonous peroxide-generating capacity) of toxoflavin limits its use.[24]

In this paper, toxoflavin was used as a starting scaffold for the design and synthesis of a focused library diversified at position 3 (Figure 1). Effect of the different aromatic substituents on the activity towards KDM4C enzyme; proliferation of two different cell lines and finally influence on the redox and ADME properties was investigated.

2. Materials and Methods

2.1. Chemistry

General procedure: Toxoflavin based compounds were synthesized by a procedure described by Todorovic *et al*.[25]
6-chloro-3-methyl-1*H*-pyrimidine-2,4-dione **(1)** (1 eq) was dissolved in EtOH (2 mL) followed by addition of methylhydrazine (2.2 eq). The reaction vessel was sealed and submitted to microwave irradiation for 10 minutes at 100°C to obtain product **2** without isolation. Aldehyde was added to the reaction mixture and again submitted to microwave irradiation for 10 minutes at 100°C. The reaction mixture was cooled to room temperature and filtered off. The resulting precipitate was washed with methanol, then diethyl ether and dried *in vacuo* to give title product **3**.

Product **3** (1 eq; 1 mmol) was dissolved in a mixture of acetic acid (7 mL) and water (0.7 mL). The reaction mixture was cooled to 0°C and sodium nitrite (1.5 eq) was added. After 6-18 hours, the reaction mixture was diluted with water and extracted with DCM. Organic layers were combined, dried over sodium sulphate, filtered and evaporated under reduced pressure to obtain crude product. Crude product was purified by flash chromatography on a silica column. The gradient was set to 0-10% MeOH/EtOAc in 25 column volumes. Appropriate fractions were combined and evaporated under reduced pressure to obtain cyclic product **4**.

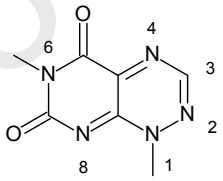

Figure 1: Numeration of toxoflavin scaffold.

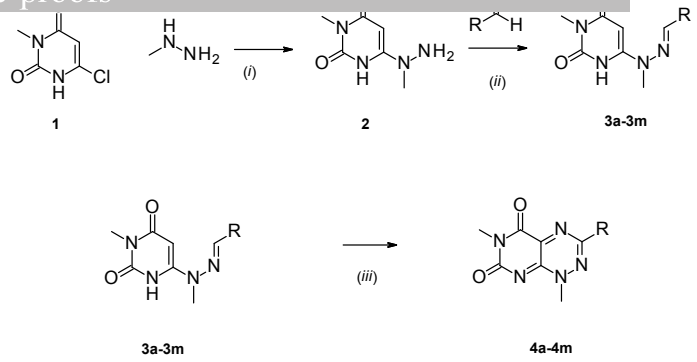

Scheme 1. Synthetic route for the preparation of focused toxoflavin library; (i): methylhydrazine, EtOH, μW, 100°C, 10 min; (ii): aldehyde, EtOH, μW, 100°C, 10 min, y=26-89%; (iii): $NaNO_2$, acetic acid/water, 0°C to RT, y=15-78%.

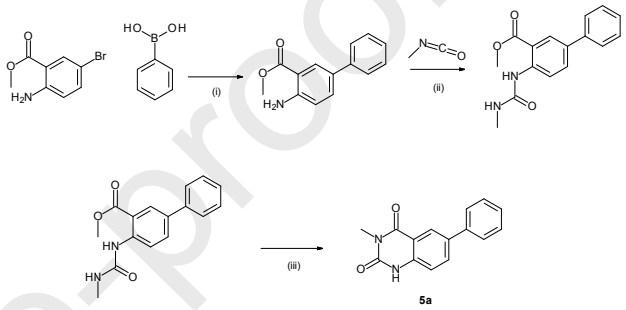

Scheme 2. Synthetic route for the preparation of novel scaffold **5a**; (i): $Pd(PPh_3)_4$, Na_2CO_3, μW, 100°C, 30 min, y=82%; (ii): DMF, 0°C to RT, y=78%; (iii): NaOEt, EtOH, 60°C, y=73%.

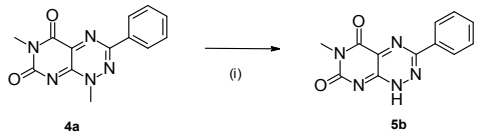

Scheme 3. Synthetic route for the preparation of novel scaffold **5b**; (i): DMF, 50°C, y=92%.

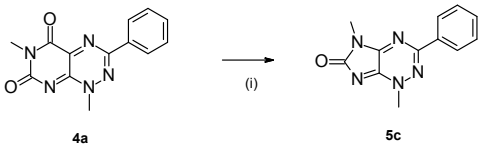

Scheme 4. Synthetic route for the preparation of novel scaffold **5c;** (i): NaOH, 10% in H_2O, 60°C, y=63%

2.1.1. (6-[[(*E*)-benzylideneamino]-methyl-amino]-3-methyl-1*H*-pyrimidine-2,4-dione, (**3a**): 6-chloro-3-methyl-1*H*-pyrimidine-2,4-dione (1 eq; 100 mg) was dissolved in EtOH (2 mL) and therafter methylhydrazine (2.2 eq; 72.06 μL) was added. The reaction vessel was sealed and submitted to microwave irradiation for 10 minutes at 100°C. Then benzaldehyde (1.6 eq; 105.75 mg) was added to the reaction mixture and again submitted to microwave irradiation for 10 minutes at 100°C. The reaction mixture was cooled to room temperature and filtered off. The resulting precipitate was washed with methanol, then diethyl ether and dried in vacuo to give title product **3a** in 89% yield; purity 100% by UPLC (UV, 254 nm). ^{1}H NMR (DMSO-*d*6, 500 MHz, δ

ppm 7.97 (s, 1H), 7.98 (s, 2H), 10.66 (s, 1H). ESI$^+$: (M+H)$^+$=259.52 m/z.

2.1.2. **(**4-[(*E*)-[methyl-(3-methyl-2,4-dioxo-1*H*-pyrimidin-6-yl)hydrazono]methyl]benzonitrile, **(3b)**: 6-chloro-3-methyl-1*H*-pyrimidine-2,4-dione (1 eq; 100 mg) was dissolved in EtOH (2 mL) and therafter methylhydrazine (2.2 eq; 72.06 µL) was added. The reaction vessel was sealed and submitted to microwave irradiation for 10 minutes at 100°C. Then 4-formylbenzonitrile (1.6 eq; 130.67 mg) was added to the reaction mixture and again submitted to microwave irradiation for 10 minutes at 100°C. The reaction mixture was cooled to room temperature and filtered off. The resulting precipitate was washed with methanol, then diethyl ether and dried in vacuo to give title product **3b** in 72% yield; purity 100% by UPLC (UV, 254 nm). ^{1}H NMR (DMSO-*d*6, 500 MHz, δ ppm): 3.11 (s, 3H), 3.37 (s, 3H), 5.30 (s, 1H), 7.88 (d, 2H, *J*=8.0 Hz), 8.01 (s, 1H), 8.19 (d, 2H, *J*=8.11 Hz), 10.93 (s, 1H). ESI$^+$: (M+H)$^+$=284.51 m/z.

2.1.3. (6-[[(*E*)-(4-hydroxyphenyl)methyleneamino]-methyl-amino]-3-methyl-1*H*-pyrimidine-2,4-dione, (**3c**): 6-chloro-3-methyl-1*H*-pyrimidine-2,4-dione (1 eq; 100 mg) was dissolved in EtOH (2 mL) and therefer methylhydrazine (2.2 eq; 72.06 µL) was added. The reaction vessel was sealed and submitted to microwave irradiation for 10 minutes at 100°C. 4-hydroxybenzaldehyde (1.6 eq; 121.91 mg) was added to the reaction mixture and again submitted to microwave irradiation for 10 minutes at 100°C. The reaction mixture was cooled to room temperature and filtered off. The resulting precipitate was washed with methanol, then diethylether and dried in vacuo to give title product **3c** in 61% yield; purity 100% by UPLC (UV, 254 nm). ^{1}H NMR (DMSO-*d*6, 500 MHz, δ ppm): 3.11 (s, 3H), 3.31 (s, 3H), 5.18 (s, 1H), 6.80 (d, 2H, *J*=8.2 Hz), 7.80 (d, 2H, *J*=8.2 Hz), 7.89 (s, 1H), 9.83 (s, 1H), 10.50 (s, 1H). ESI$^+$: (M+H)$^+$=275.51 m/z.

2.1.4. 4(6-[[(*E*)-(4-methoxyphenyl)methyleneamino]-methyl-amino]-3-methyl-1*H*-pyrimidine-2,4-dione, (**3d**): 6-chloro-3-methyl-1*H*-pyrimidine-2,4-dione (1 eq; 100 mg) was dissolved in EtOH (2 mL) and therafter methylhydrazine (2.2 eq; 72.06 µL) was added. The reaction vessel was sealed and submitted to microwave irradiation for 10 minutes at 100°C. 4-methoxybenzaldehyde (1.6 eq; 135.67 mg) was added to the reaction mixture and again submitted to microwave irradiation for 10 minutes at 100°C. The reaction mixture was cooled to room temperature and filtered off. The resulting precipitate was washed with methanol, then diethyl ether and dried in vacuo to give title product **3d** in 87% yield; purity 99% by UPLC (UV, 254 nm). ^{1}H NMR (DMSO-*d*6, 500 MHz, δ ppm): 3.11 (s, 3H), 3.80 (s, 3H), 5.19 (s, 1H), 6.99 (d, 2H, *J*=8.44 Hz), 7.90-7.95 (m, 3H), 10.60 (s, 1H). ESI$^+$: (M+H)$^+$=289.58 m/z.

2.1.5. (4-[(*E*)-[methyl-(3-methyl-2,4-dioxo-1*H*-pyrimidin-6-yl)hydrazono]methyl]benzenesulfonamide, (**3e**): 6-chloro-3-methyl-1*H*-pyrimidine-2,4-dione (1 eq; 100 mg) was dissolved in EtOH (2 mL) and theafter methylhydrazine (2.2 eq; 72.06 µL) was added. The reaction vessel was sealed and submitted to microwave irradiation for 10 minutes at 100°C. 4-formylbenzenesulfonamide (1.6 eq; 184.56 mg) was added to the reaction mixture and again submitted to microwave irradiation for 10 minutes at 100°C. The reaction mixture was cooled to room temperature and filtered off. The resulting precipitate was washed with methanol, then diethyl ether and dried in vacuo to give title product **3e** in 34% yield; purity 100% by UPLC (UV, 254 nm). ^{1}H NMR (DMSO-*d*6, 500 MHz, δ ppm): 3.12 (s, 3H), 3.37 (s, 3H), 5.29 (s, 1H), 7.41 (s, 2H), 7.85 (d, 2H, *J*=8.1 Hz), 8.02 (s, 1H), 8.17 (d, 2H, *J*=8.1 Hz), 10.85 (s, 1H). ESI$^+$: (M+H)$^+$=338.51 m/z.

2.1.6. (methyl-[4-[(*E*)-[methyl-(3-methyl-2,4-dioxo-1*H*-pyrimidin-6-yl)hydrazono]methyl]phenyl]cyclopropanecarboxylate, (**3f**): 6- was dissolved in EtOH (2 mL) and thereafter methylhydrazine (2.2 eq; 72.06 µL) was added. The reaction vessel was sealed and submitted to microwave irradiation for 10 minutes at 100°C. Methyl 1-(4-formylphenyl)cyclopropanecarboxylate (1.6 eq; 203.51 mg) was added to the reaction mixture and again submitted to microwave irradiation for 10 minutes at 100°C. The reaction mixture was cooled to room temperature and filtered off. The resulting precipitate was washed with methanol, then diethyl ether and dried in vacuo to give title product **3f** in 62% yield; purity 100% by UPLC (UV, 254 nm). ^{1}H NMR (DMSO-*d*6, 500 MHz, δ ppm): 1.22 (s, 2H), 1.50 (s, 2H), 3.11 (s, 3H), 3.34 (s, 3H), 3.55 (s, 3H), 5.24 (s, 1H), 7.38 (d, 2H, *J*=8.22 Hz), 7.90 (d, 2H, *J*=7.76 Hz), 7.97 (s, 1H), 10.65 (s, 1H). ESI$^+$: (M+H)$^+$=357.61 m/z.

2.1.7.(3-methyl-6-[methyl-[(*E*)-2-phenylethylideneamino]amino]-1*H*-pyrimidine-2,4-dione, (**3g**): 6-chloro-3-methyl-1*H*-pyrimidine-2,4-dione (1 eq; 100 mg) was dissolved in EtOH (2 mL) and therafter methylhydrazine (2.2 eq; 72.06 µL) was added. The reaction vessel was sealed and submitted to microwave irradiation for 10 minutes at 100°C. 2-phenylacetaldehyde (1.6 eq; 119.72 mg) was added to the reaction mixture and again submitted to microwave irradiation for 10 minutes at 100°C. The reaction mixture was cooled to room temperature and filtered off. The resulting precipitate was washed with methanol, then diethyl ether and dried in vacuo to give title product **3g** in 63% yield; purity 99% by UPLC (UV, 254 nm). ^{1}H NMR (DMSO-*d*6, 500 MHz, δ ppm): 3.09 (s, 3H), 3.15 (s, 3H), 3.71 (d, 2H, *J*=5.4 Hz), 5.11 (s, 1H), 7.20-7.26 (m, 1H), 7.26-7.35 (m, 5H), 10.41 (s, 1H). ESI$^+$: (M+H)$^+$=273.55 m/z.

2.1.8. 8(6-[[(*E*)-1*H*-indol-3-ylmethyleneamino]-methyl-amino]-3-methyl-1*H*-pyrimidine-2,4-dione, (**3h**): 6-chloro-3-methyl-1*H*-pyrimidine-2,4-dione (1 eq; 100 mg) was dissolved in EtOH (2 mL) and thereafter methylhydrazine (2.2 eq; 72.06 µL) was added. The reaction vessel was sealed and submitted to microwave irradiation for 10 minutes at 100°C. 1*H*-indole-3-carbaldehyde (1.6 eq; 169.57 mg) was added to the reaction mixture and again submitted to microwave irradiation for 10 minutes at 100°C. The reaction mixture was cooled to room temperature and filtered off. The resulting precipitate was washed with methanol, then diethyl ether and dried in vacuo to give title product **3h** in 28% yield; purity 100% by UPLC (UV, 254 nm). ^{1}H NMR (DMSO-*d*6, 500 MHz, δ ppm): 3.12 (s, 3H), 3.36 (s, 3H), 5.24 (s, 1H), 7.14-7.24 (m, 2H), 7.47 (d, 1H, *J*=7.75 Hz), 7.97 (s, 1H), 8.03 (d, 1H, *J*=7.55 Hz), 8.25 (s, 1H), 10.05 (s, 1H), 11.62 (s, 1H). ESI$^+$: (M+H)$^+$=298.56 m/z.

2.1.9. (3-methyl-6-[methyl-[(*E*)-1*H*-pyrrolo[2,3-*b*]pyridin-3-ylmethyleneamino]amino]-1*H*-pyrimidine-2,4-dione, (**3i**): 6-chloro-3-methyl-1*H*-pyrimidine-2,4-dione (1 eq; 100 mg) was dissolved in EtOH (2 mL) and therafter methylhydrazine (2.2 eq; 72.06 µL) was added. The reaction vessel was sealed and submitted to microwave irradiation for 10 minutes at 100°C. 1*H*-pyrrolo[2,3-*b*]pyridine-3-carbaldehyde(1.6 eq; 145.63 mg) was added to the reaction mixture and again submitted to microwave irradiation for 10 minutes at 100°C. The reaction mixture was cooled to room temperature and filtered off. The resulting precipitate was washed with methanol, then diethylether and dried in vacuo to give title product **3i** in 26% yield; purity 95% by UPLC (UV, 254 nm). ^{1}H NMR (DMSO-*d*6, 500 MHz, δ ppm): 3.12 (s, 3H), 3.36 (s, 3H), 5.23 (s, 1H), 7.23 (m, 1H), 8.11 (s, 1H), 8.22 (s, 1H), 8.29-8.32 (m, 1H), 8.41 (d, 1H, *J*=8.07 Hz), 10.25 (s, 1H), 12.14 (s, 1H). ESI$^+$: (M+H)$^+$=299.56 m/z.

2.1.10. (3-methyl-6-[methyl-[(*E*)-4-pyridylmethyleneamino]amino]-1*H*-pyrimidine-2,4-dione, (**3j**): 6-chloro-3-methyl-1*H*-pyrimidine-2,4-dione (1 eq; 100 mg) was dissolved in EtOH (2 mL) and therafter methylhydrazine (2.2 eq; 72.06 µL) was added. The reaction vessel was sealed and

submitted to microwave irradiation for 10 minutes at 100°C. 10% Pyridine-4-carbaldehyde (1.6 eq; 106.74 mg) was added to the reaction mixture and again submitted to microwave irradiation for 10 minutes at 100°C. The reaction mixture was cooled to room temperature and filtered off. The resulting precipitate was washed with methanol, then diethyl ether and dried in vacuo to give title product **3j** in 45% yield; purity 99% by UPLC (UV, 254 nm). ^{1}H NMR (DMSO-*d*6, 500 MHz, δ ppm): 3.12 (s, 3H), 3.37 (s, 3H), 5.32 (s, 1H), 7.92-7.97 (m, 3H), 8.62 (d, 2H, *J*=4.57 Hz), 10.91 (s, 1H). ESI$^+$: (M+H)$^+$=260.54 m/z.

2.1.11. (3-methyl-6-[methyl-[(*E*)-(1-methyl-2-oxo-4-pyridyl)methyleneamino]amino]-1*H*-pyrimidine-2,4-dione, (**3k**): 6-chloro-3-methyl-1H-pyrimidine-2,4-dione (1 eq; 100 mg) was dissolved in EtOH (2 mL) and thereafter methylhydrazine (2.2 eq; 72.06 µL) was added. The reaction vessel was sealed and submitted to microwave irradiation for 10 minutes at 100°C. 1-methyl-2-oxo-pyridine-4-carbaldehyde (1.6 eq; 136.65 mg) was added to the reaction mixture and again submitted to microwave irradiation for 10 minutes at 100°C. The reaction mixture was cooled to room temperature and filtered off. The resulting precipitate was washed with methanol, then diethyl ether and dried in vacuo to give title product **3k** in 41% yield; purity 94% by UPLC (UV, 254 nm). ^{1}H NMR (DMSO-*d*6, 500 MHz, δ ppm): 3.11 (s, 3H), 3.31 (s, 3H), 3.49 (s, 3H), 5.23 (s, 1H), 6.32-6.37 (m, 1H), 7.82 (d, 1H, *J*=6.62 Hz), 7.94 (s, 1H), 8.54 (d, 1H, *J*=7.16 Hz), 10.71 (s, 1H). ESI$^+$: (M+H)$^+$=290.53 m/z.

2.1.12. (6-[[(*E*)-[2-(dimethylamino)phenyl]methyleneamino]-methyl-amino]-3-methyl-1*H*-pyrimidine-2,4-dione, (**3l**): 6-chloro-3-methyl-1*H*-pyrimidine-2,4-dione (1 eq; 100 mg) was dissolved in EtOH (2 mL) and thereafter methylhydrazine (2.2 eq; 72.06 µL) was added. The reaction vessel was sealed and submitted to microwave irradiation for 10 minutes at 100°C. 2-(dimethylamino)benzaldehyde (1.6 eq; 148.66 mg) was added to the reaction mixture and again submitted to microwave irradiation for 10 minutes at 100°C. The reaction mixture was cooled to room temperature and filtered off. The resulting precipitate was washed with methanol, then diethylether and dried in vacuo to give title product **3l** in 38% yield; purity 100% by UPLC (UV, 254 nm). ^{1}H NMR (DMSO-*d*6, 500 MHz, δ ppm): 2.70 (s, 6H), 3.11 (s, 3H), 3.36 (s, 3H), 5.26 (s, 1H), 7.06 (t, 1H, *J*=7.56 Hz), 7.13 (d, 1H, *J*=8.14 Hz), 7.34 (t, 1H, *J*=7.85 Hz), 8.03 (s, 1H), 8.19 (d, 1H, *J*=7.85 Hz), 10.56 (s, 1H). ESI$^+$: (M+H)$^+$=302.59 m/z.

2.1.13. (6-[[(*E*)-(4-fluorophenyl)methyleneamino]-methyl-amino]-3-methyl-1*H*-pyrimidine-2,4-dione, (**3m**): 6-chloro-3-methyl-1*H*-pyrimidine-2,4-dione (1 eq; 100 mg) was dissolved in EtOH (2 mL) and thereafter methylhydrazine (2.2 eq; 72.06 µL) was added. The reaction vessel was sealed and submitted to microwave irradiation for 10 minutes at 100°C. 4-fluorobenzaldehyde (1.6 eq; 123.68 mg) was added to the reaction mixture and again submitted to microwave irradiation for 10 minutes at 100°C. The reaction mixture was cooled to room temperature and filtered off. The resulting precipitate was washed with methanol, then diethyl ether and dried in vacuo to give title product **3m** in 60% yield; purity 100% by UPLC (UV, 254 nm). ^{1}H NMR (DMSO-*d*6, 500 MHz, δ ppm): 3.11 (s, 3H), 3.34 (s, 3H), 5.23 (s, 1H), 7.23-7.29 (m, 2H), 7.98 (s, 1H), 8.06 (m, 2H), 10.76 (s, 1H). ESI$^+$: (M+H)$^+$=277.53 m/z.

2.1.14. (1,6-dimethyl-3-phenyl-pyrimido[5,4-*e*][1,2,4]triazine-5,7-dione, (**4a**): 6-[[(*E*)-benzylideneamino]-methyl-amino]-3-methyl-1*H*-pyrimidine-2,4-dione (1 eq; 1 mmol) was dissolved in a mixture of acetic acid (7 mL) and water (0.7 mL). The reaction mixture was cooled to 0°C and sodium nitrite (1.5 eq) was added. After 6 hours, the reaction mixture was diluted with water and extracted with DCM. Organic layers were combined, dried over sodium sulphate, filtered and evaporated under reduced pressure to obtain crude product. Crude product was purified by flash chromatography on silica column. The gradient was set to 0-10% MeOH/EtOAc. Appropriate fractions were combined and evaporated under reduced pressure to obtain title product **4a** in 78% yield, purity 94% by UPLC (UV, 254 nm). ^{1}H NMR (DMSO-*d*6, 500 MHz, δ ppm): 3.29 (s, 3H), 4.06 (s, 3H), 7.59 (s, 3H), 8.20 (s, 2H). ^{13}C NMR (DMSO-*d*6, 150 MHz, δ ppm): 28.3, 43.3, 127.0, 127.5, 129.6, 131.7, 134.8, 149.9, 150.5, 160.2, 161.2. ESI$^+$: (M+H)$^+$=270,50 m/z. UV: λ_{max} (MeCN)=282 nm; 298 nm. Published by Kyani *et al.*[26]

2.1.15. (4-(1,6-dimethyl-5,7-dioxo-pyrimido[5,4-*e*][1,2,4]triazin-3-yl)benzonitrile, (**4b**): 4-[(*E*)-[methyl-(3-methyl-2,4-dioxo-1*H*-pyrimidin-6-yl)hydrazono]methyl]benzonitrile(1 eq; 1 mmol) was dissolved in a mixture of acetic acid (7 mL) and water (0.7 mL). The reaction mixture was cooled to 0°C and sodium nitrite (1.5 eq) was added. After 6 hours, the reaction mixture was diluted with water and extracted with DCM. Organic layers were combined, dried over sodium sulphate, filtered and evaporated under reduced pressure to obtain crude product. Crude product was purified by flash chromatography on silica column. The gradient was set to 0-10% MeOH/EtOAc. Appropriate fractions were combined and evaporated under reduced pressure to obtain title product **4b** in 22% yield, purity 96% by UPLC (UV, 254 nm). ^{1}H NMR (DMSO-*d*6, 500 MHz, δ ppm): 3.27 (s, 3H), 4.06 (s, 3H), 8.07 (s, 2H), 8.34 (s, 2H). ESI$^+$: (M+H)$^+$=295.54 m/z. UV: λ_{max} (MeCN) =285 nm; 298 nm. Published by Todorovic *et al.*[25]

2.1.16. (3-(4-hydroxyphenyl)-1,6-dimethyl-pyrimido[5,4-*e*][1,2,4]triazine-5,7-dione, (**4c**): 6-[[(*E*)-(4-hydroxyphenyl)methyleneamino]-methyl-amino]-3-methyl-1*H*-pyrimidine-2,4-dione(1 eq; 1 mmol) was dissolved in a mixture of acetic acid (7 mL) and water (0.7 mL). The reaction mixture was cooled to 0°C and sodium nitrite (1.5 eq) was added. After 6 hours, the reaction mixture was diluted with water and extracted with DCM. Organic layers were combined, dried over sodium sulphate, filtered and evaporated under reduced pressure to obtain crude product. Crude product was purified by flash chromatography on silica column. Gradient was set 0-10% MeOH/EtOAc. Appropriate fractions were combined and evaporated under reduced pressure to obtain title product **4c** in 28% yield, purity 85% by UPLC (UV, 254 nm). ^{1}H NMR (DMSO-*d*6, 500 MHz, δ ppm): 3.27 (s, 3H), 4.01 (s, 3H), 6.94 (d, 2H, *J*=7.83 Hz), 8.03 (d, 2H, *J*=8.17 Hz), 10.17 (s, 1H). ESI$^+$: (M+H)$^+$=286.51 m/z. UV: λ_{max} (MeCN) =227 nm. Published by Zeller *et al.*[27]

2.1.17. (3-(4-methoxyphenyl)-1,6-dimethyl-pyrimido[5,4-*e*][1,2,4]triazine-5,7-dione, (**4d**): 6-[[(*E*)-(4-methoxyphenyl)methyleneamino]-methyl-amino]-3-methyl-1*H*-pyrimidine-2,4-dione (1 eq; 1 mmol) was dissolved in a mixture of acetic acid (7 mL) and water (0.7 mL). The reaction mixture was cooled to 0°C and sodium nitrite (1.5 eq) was added. After 6 hours, the reaction mixture was diluted with water and extracted with DCM. Organic layers were combined, dried over sodium sulphate, filtered and evaporated under reduced pressure to obtain crude product. Crude product was purified by flash chromatography on silica column. Gradient was set 0-10% MeOH/EtOAc. Appropriate fractions were combined and evaporated under reduced pressure to obtain title product **4d** in 15% yield, purity 92% by UPLC (UV, 254 nm). ^{1}H NMR (DMSO-*d*6, 500 MHz, δ ppm): 3.27 (s, 3H), 3.85 (s, 3H), 4.03 (s, 3H), 7.14 (d, 2H, *J*=8.65 Hz), 8.13 (d, 2H, *J*=8.37 Hz). ^{13}C NMR (DMSO-*d*6, 150 MHz, δ ppm): 28.7, 43.2, 55.9, 115.2, 125.5, 128.8, 146.8, 149.7, 151.7, 154.5, 159.5, 162.3. ESI$^+$: (M+H)$^+$=300.53 m/z. UV: λ_{max} (MeCN) =305 nm. Published by Zeller *et al.*[27]

2.1.18. 4-(1,6-dimethyl-5,7-dioxo-pyrimido[5,4-*e*][1,2,4]triazin-3-yl)benzenesulfonamide, (**4e**): 4-[(*E*)-[methyl-(3-methyl-2,4-dioxo-1*H*-pyrimidin-6-yl)hydrazono]methyl]benzenesulfonamide(1 eq; 1mmol) was

dissolved in a mixture of acetic acid (7 mL) and water (0.7 mL). The reaction mixture was cooled to 0°C and sodium nitrite (1.5 eq) was added. After 6 hours, the reaction mixture was diluted with water and extracted with DCM. Organic layers were combined, dried over sodium sulphate, filtered and evaporated under reduced pressure to obtain crude product. Crude product was purified by flash chromatography on silica column. The gradient was set to 0-10% MeOH/EtOAc. Appropriate fractions were combined and evaporated under reduced pressure to obtain title product **4e** in 17% yield, purity 89% by UPLC (UV, 254 nm). ^{1}H NMR (DMSO-*d*6, 500 MHz, δ ppm): 3.29 (s, 3H), 4.07 (s, 3H), 7.54 (s, 2H), 8.03 (d, 2H, *J*=8.30 Hz), 8.36 (d, 2H, *J*=8.30 Hz). ESI$^+$: (M+H)$^+$=349.54 m/z. UV: λ_{max} (MeCN) =234 nm; 296 nm.

2.1.19. (methyl-1-[4-(1,6-dimethyl-5,7-dioxo-pyrimido[5,4-*e*][1,2,4]triazin-3-yl)phenyl]cyclopropanecarboxylate, (**4f**): methyl 1-[4-[(*E*)-[methyl-(3-methyl-2,4-dioxo-1*H*-pyrimidin-6-yl)hydrazono]methyl]phenyl]cyclopropanecarboxylate(1 eq; 1 mmol) was dissolved in a mixture of acetic acid (7 mL) and water (0.7 mL). The reaction mixture was cooled to 0°C and sodium nitrite (1.5 eq) was added. After 6 hours, the reaction mixture was diluted with water and extracted with DCM. Organic layers were combined, dried over sodium sulphate, filtered and evaporated under reduced pressure to obtain crude product. Crude product was purified by flash chromatography on silica column. The gradient was set to 0-10% MeOH/EtOAc. Appropriate fractions were combined and evaporated under reduced pressure to obtain title product **4f** in 21% yield, purity 99% by UPLC (UV, 254 nm). ^{1}H NMR (DMSO-*d*6, 500 MHz, δ ppm): 1.27 (s, 2H), 1.54 (s, 2H), 3.28 (s, 3H), 3.57 (s, 3H), 4.05 (s, 3H), 7.55 (d, 2H, *J*=7.89 Hz), 8.12 (d, 2H, *J*=7.89 Hz). ESI$^+$: (M+H)$^+$=368.60 m/z. UV: λ_{max} (MeCN)=282 nm; 304 nm.

2.1.20. (3-benzyl-1,6-dimethyl-pyrimido[5,4-*e*][1,2,4]triazine-5,7-dione, (**4g**): 3-methyl-6-[methyl-[(*E*)-2-phenylethylideneamino]amino]-1*H*-pyrimidine-2,4-dione (1 eq; 1 mmol) was dissolved in a mixture of acetic acid (7 mL) and water (0.7 mL). The reaction mixture was cooled to 0°C and sodium nitrite (1.5 eq) was added. After 6 hours, the reaction mixture was diluted with water and extracted with DCM. Organic layers were combined, dried over sodium sulphate, filtered and evaporated under reduced pressure to obtain crude product. Crude product was purified by flash chromatography on silica column. The gradient was set to 0-10% MeOH/EtOAc. Appropriate fractions were combined and evaporated under reduced pressure to obtain title product **4g** in 38% yield, purity 85% by UPLC (UV, 254 nm). ^{1}H NMR (DMSO-*d*6, 500 MHz, δ ppm): 3.23 (s, 3H), 3.93 (s, 3H), 4.22 (s, 1H), 4.46 (s, 1H), 7.20-7.34 (m, 5H). ^{13}C NMR (DMSO-*d*6, 150 MHz, δ ppm): 28.2, 28.7, 42.6, 127.1, 129.0, 129.5, 138.2, 150.0, 150.4, 155.8, 161.1, 165.0. ESI$^+$: (M+H)$^+$=284.51 m/z. UV: λ_{max} (MeCN) =264 nm. Published by Kyani *et al.*[26]

2.1.21.(1,6-dimethyl-3-(4-pyridyl)pyrimido[5,4-*e*][1,2,4]triazine-5,7-dione, (**4j**): 3-methyl-6-[methyl-[(*E*)-4-pyridylmethyleneamino]amino]-1*H*-pyrimidine-2,4-dione (1 eq; 1 mmol) was dissolved in a mixture of acetic acid (7 mL) and water (0.7 mL). The reaction mixture was cooled to 0°C and sodium nitrite (1.5 eq) was added. After 6 hours, the reaction mixture was diluted with water and extracted with DCM. Organic layers were combined, dried over sodium sulphate, filtered and evaporated under reduced pressure to obtain crude product. Crude product was purified by flash chromatography on silica column. The gradient was set to 0-10% MeOH/EtOAc. Appropriate fractions were combined and evaporated under reduced pressure to obtain title product **4j** in 26% yield, purity 91% by UPLC (UV, 254 nm). ^{1}H NMR (DMSO-*d*6, 500 MHz, δ ppm): 3.29 (s, 3H), 4.07 (s, 3H), 8.08 (s, 2H), 8.82 (s, 2H). ESI$^+$: (M+H)$^+$=271,53 m/z. UV: λ_{max} (MeCN) =284 nm.

2,3,5lambda5,8,10-pentazabicyclo[4.4.0]deca-1(10),3,5-triene-7,9-dione, (**4k**): 3-methyl-6-[methyl-[(*E*)-(1-methyl-2-oxo-4-pyridyl)methyleneamino]amino]-1*H*-pyrimidine-2,4-dione (1 eq; 1 mmol) was dissolved in a mixture of acetic acid (7 mL) and water (0.7 mL). The reaction mixture was cooled to 0°C and sodium nitrite (1.5 eq) was added. After 6 hours, the reaction mixture was diluted with water and extracted with DCM. Organic layers were combined, dried over sodium sulphate, filtered and evaporated under reduced pressure to obtain crude product. Crude product was purified by flash chromatography on silica column. The gradient was set to 0-10% MeOH/EtOAc. Appropriate fractions were combined and evaporated under reduced pressure to obtain title product **4k** in 32% yield, purity 97% by UPLC (UV, 254 nm). ^{1}H NMR (DMSO-*d*6, 500 MHz, δ ppm): 3.17 (s, 3H), 3.50 (s, 3H), 3.84 (s, 3H), 6.39 (m, 1H), 7.68 (d, 2H, *J*=7.07 Hz), 7.99 (d, 2H, *J*=6.39 Hz). ESI$^+$: (M+H)$^+$=317.54 m/z. UV: λ_{max} (MeCN) =265 nm; 321 nm.

2.1.23 .(3-[2-(dimethylamino)phenyl]-1,6-dimethyl-pyrimido[5,4-*e*][1,2,4]triazine-5,7-dione, (**4l**): 6-[[(*E*)-[2-(dimethylamino)phenyl]methyleneamino]-methyl-amino]-3-methyl-1*H*-pyrimidine-2,4-dione (1 eq; 1 mmol) was dissolved in a mixture of acetic acid (7 mL) and water (0.7mL). The reaction mixture was cooled to 0°C and sodium nitrite (1.5 eq) was added. After 6 hours, the reaction mixture was diluted with water and extracted with DCM. Organic layers were combined, dried over sodium sulphate, filtered and evaporated under reduced pressure to obtain crude product. Crude product was purified by flash chromatography on silica column. The gradient was set to 0-10% MeOH/EtOAc. Appropriate fractions were combined and evaporated under reduced pressure to obtain title product **4l** in 43% yield, purity 91% by UPLC (UV, 254 nm). ^{1}H NMR (DMSO-*d*6, 500 MHz, δ ppm): 2.55 (s, 3H), 2.65 (s, 3H), 3.27 (s, 3H), 4.01 (s, 3H), 6.97-7.05 (m, 1H), 7.08-7.15 (m, 1H), 7.38-7.48 (m, 2H). ESI$^+$: (M+H)$^+$=313.57 m/z. UV: λ_{max} (MeCN) =239 nm.

2.1.24. (3-(4-fluorophenyl)-1,6-dimethyl-pyrimido[5,4-*e*][1,2,4]triazine-5,7-dione, (**4m**): 6-[[(*E*)-(4-fluorophenyl)methyleneamino]-methyl-amino]-3-methyl-1*H*-pyrimidine-2,4-dione (1 eq; 1 mmol) was dissolved in a mixture of acetic acid (7 mL) and water (0.7 mL). The reaction mixture was cooled to 0°C and sodium nitrite (1.5 eq) was added. After 6 hours, the reaction mixture was diluted with water and extracted with DCM. Organic layers were combined, dried over sodium sulphate, filtered and evaporated under reduced pressure to obtain crude product. Crude product was purified by flash chromatography on silica column. The gradient was set to 0-10% MeOH/EtOAc. Appropriate fractions were combined and evaporated under reduced pressure to obtain title product **4m** in 62% yield, purity 100% by UPLC (UV, 254 nm). ^{1}H NMR (DMSO-*d*6, 500 MHz, δ ppm): 3.28 (s, 3H), 4.05 (s, 3H), 7.39-7.48 (m, 2H), 8.19-8.28 (m, 2H). ESI$^+$: (M+H)$^+$=288.51 m/z. UV: λ_{max} (MeCN) =285 nm. Published by Todorovic *et al.*[25]

2.1.25. 3-methyl-6-phenyl-1H-quinazoline-2,4-dione, **(5a)**: **Step 1**: The reaction vessel was charged with methyl 2-amino-5-bromo-benzoate (200 mg), phenylboronic acid (106 mg), Na_2CO_3 (276.40 mg) and $Pd(PPh_3)_4$ (100.46 mg). 1,4-dioxane (3 mL) and water (1 mL) were added. The reaction vessel was sealed, vacuumed, backfilled with argon and submitted to microwave irradiation for 30 minutes at 100°C. The reaction mixture was diluted with water and extracted with DCM. Organic layers were combined, dried over sodium sulphate, filtered and evaporated under reduced pressure to obtain crude product. Crude product was purified by flash chromatography on silica column. The gradient was set to 0-50% EtOAc/cyclohexane in 25 CVs. Appropriate fractions were combined and evaporated under reduced pressure to obtain intermediate **5i;** methyl 2-amino-5-phenyl-benzoate in 82% yield,

purified by flash chromatography on silica column. The gradient was set to 0-50% EtOAc/cyclohexane in 25 CVs. Appropriate fractions were combined and evaporated under reduced pressure to obtain product **5i** methyl 2-(methylcarbamoylamino)-5-phenyl-benzoate in 77% yield, purity 75% by UPLC (UV, 254 nm). **Step 2**: Methyl 2-(methylcarbamoylamino)-5-phenyl-benzoate (**5i**) (200 mg) was dissolved in dry DMF (2 mL). The reaction mixture was cooled to 0°C, methylimino(oxo)methane (106 mg) was added and allowed to slowly warm to room temperature. After 3 hours, the reaction was diluted with water and extracted with EtOAc. Organic layers were combined, dried over sodium sulphate, filtered and evaporated under reduced pressure to obtain crude product. Crude product was purified by flash chromatography on silica column. The gradient was set to 0-50% EtOAc/cyclohexane in 25 CVs. Appropriate fractions were combined and evaporated under reduced pressure to obtain intermediate **5ii** methyl 2-(methylcarbamoylamino)-5-phenyl-benzoate in 77% yield, purity 75% by UPLC (UV, 254 nm). **Step 3**: Methyl 2-(methylcarbamoylamino)-5-phenyl-benzoate (**5ii**) (20 mg) was dissolved in NaOEt, 20% solution in ethanol. Reaction mixture was heated to 60°C. After 3 hours reaction mixture was cooled to room temperature, diluted with water and extracted with DCM. Organic layers were combined, dried over sodium sulphate, filtered and evaporated under reduced pressure to obtain crude product. Crude product was purified by flash chromatography using silica column. Gradient was set 0-50% EtOAc/cyclohexane in 25 CVs. Appropriate fractions were combined and evaporated under reduced pressure to obtain product **5a,** 3-methyl-6-phenyl-1*H*-quinazoline-2,4-dione in 73% yield, purity 95% by UPLC (UV, 254 nm). ^{1}H NMR (DMSO-*d*6, 500 MHz, δ ppm): 3.28 (s,3H), 7.27 (d, 1H, *J*=5.06Hz), 7.37 (t, 1H, *J*=7.45Hz), 7.48 (t, 2H, *J*=7.45 Hz), 7.68 (d, 2H, *J*=3.99 Hz), 7.98 (d, 1H, *J*=4.07 Hz), 8.14 (s, 1H), 11.51 (s, 1H). ^{13}C NMR (DMSO-*d*6, 150 MHz, δ ppm): 27.6, 114.6, 116.4, 125.0, 126.8, 128.0, 129.6, 133.7, 134.9, 139.1, 139.2, 150.7, 162.6. ESI^{+}: $(M+H)^{+}$=253.14 m/z. UV: λ_{max} (MeCN) =236 nm; 268 nm.

2.1.26. 6-methyl-3-phenyl-1*H*-pyrimido[5,4-*e*][1,2,4]triazine-5,7-dione, (**5b**): Method described by Nagamatsu *et al.*[28] 1,6-dimethyl-3-phenyl-pyrimido[5,4-*e*][1,2,4]triazine-5,7-dione (**4a**) was dissolved in DMF and heated to 50°C. After 3 hours, the reaction mixture was cooled to room temperature, diluted with water and extracted with DCM. Organic layers were combined, dried over sodium sulphate, filtered and evaporated under reduced pressure to obtain crude product. Crude product was purified by flash chromatography on silica column. The gradient was set to 0-10% MeOH/EtOAc. Appropriate fractions were combined and evaporeted under reduced pressure to obtain title product **5b** in 92% yield, purity 100% by UPLC(UV, 254 nm). ^{1}H NMR (DMSO-*d*6, 500 MHz, δ ppm): 3.29 (s, 3H), 7.61 (m, 3H), 8.40 (m, 2H), 12.82 (s, 1H). ESI^{+}: $(M+H)^{+}$=256.08 m/z. UV: λ_{max} (MeCN) =273 nm; 302 nm. Published by Nagamatsu *et al.*[28]

2.1.27.1,5-dimethyl-3-phenyl-imidazo[4,5-*e*][1,2,4]triazin-6-one (**5c**): Method described by Yoneda *et al.*[29] 1,6-dimethyl-3-phenyl-pyrimido[5,4-*e*][1,2,4]triazine-5,7-dione (**4a**) was dissolved in NaOH, 10% solution in water (1 mL). The reaction mixture was heated to 60°C, stirred and after 2 hours the reaction mixture was cooled to room temperature, diluted with water and extracted with DCM. Organic layers were combined, dried over sodium sulphate, filtered and evaporated under reduced pressure to obtain crude product. Crude product was purified by flash chromatography using silica column. The gradient was set to 0-10% MeOH/EtOAc. The appropriate fractions were combined and evaporeted under reduced pressure to obtain title product **5c** in 63% yield, purity 97% by UPLC (UV, 254 nm). ^{1}H NMR (DMSO-*d*6, 500 MHz, δ ppm): 3.33 (s, 3H), 3.98 (s, 3H), 7.53 (m, 3H), 8.21 (m, 2H). ESI^{+}: $(M+H)^{+}$=242.11 m/z. UV: λ_{max} (MeCN) =280 nm; 334 nm. Published by Yoneda *et al.* [29]

2.2. Biological activity evaluation *in vitro*

Newly synthetized compounds using the BPS Bioscience (San Diego, USA) biochemical assay kit. The KDM4C chemiluminescent assay kit was designed to measure activity of the KDM4C using a highly specific antibody that recognizes the demethylated substrate. The experimental procedure comprises of three steps on a microtiter plate to detect methyltransferase: 1) KDM4C enzyme was incubated with a sample containing assay buffer for one hour; 2) primary antibody was added; 3) the plate was treated with an HRP-labelled secondary antibody followed by addition of the HRP substrate to produce chemiluminescence that was measured using a chemiluminescence reader (EnVision, Perkin Elmer). Newly synthetized compounds were tested at 10 μM in primary screening, and in dose-response range in secondary screening, in order to produce IC_{50} values (10 μM starting compound concentration, 1:5 dilution), and results were presented as a IC_{50} values of the KDM4C enzyme. 2,4-pyridinedicarboxylic acid was used as a control compound with literature known activity. Assays for determination of percentage of inhibition and IC_{50} values were performed following manufacturers protocol.[30]

2.3. Influence on cell proliferation of HepG2 and A549 cell lines

2.3.1. HepG2 cell line

Proliferation of human Caucasian hepatocyte carcinoma (HepG2) cell line was investigated after 24 hour incubation with compounds by a modified version of Mosmann.[31]. A mother plate (Storplate-384- deep-well-V plate, Perkin Elmer) with 1 : 2 serial dilutions (9 concentrations; starting from 25 μM concentration) of the compounds in pure DMSO was prepared in duplicate from compound stock solutions (1 mg/mL). 500 nL of compounds solution was transferred from the mother plate to the test plate by using a nanovolume liquid handling instrument Mosquito (3019-0002, TTP Labtech). Cells were distributed in 384-well plates, at concentrations of 2×10^4 cells per well, in 50 μL of cell culture medium. Control conditions (cells/media) were spiked with equal final DMSO concentrations of 1% DMSO. Cells were incubated for 24 h at 37°C, 5% CO_2 and 95% humidity. Cell growth was estimated by the MTS [3-(4,5-dimethylthiazol-2-yl)-5-(3-carboxymethoxyphenyl)-2-(4-sulfophenyl)-2H-tetrazolium] assay. After adding 5 μL of MTS, plates were incubated for 2 hours at 37°C. Absorbance at 492 nm was measured with a plate reader. The reference control compound for MTS assay was staurosporine, which showed acceptable standard value for this assay. Data was evaluated using predefined IC_{50} equation from GraphPad Prism program, version 5.3 for Windows (GraphPad Software, San Diego, CA).

2.3.2. A549 cell line

Proliferation of adenocarcinomic human alveolar basal epithelial (A549) cell line was investigated after 72 hours of incubation with compounds. Compounds were tested in eight consecutive three-fold dilutions starting from 30 μM in duplicates placed on two different plates. Side control conditions (cells/media) were spiked with equal final DMSO concentrations of 0.3% DMSO. 100 μL of A549 cells was added, in concentration of 1×10^4 cells per well. Cells were incubated for 72 h at 37°C, 5% CO_2 and 95% humidity. Determination of proliferation inhibition was performed using Alamar blue (Invitrogen, Cat. No. DAL1100), according to the manufacturer instructions. After 72 hours, 10 μL of Alamar blue per well is added. Cells were then incubated 4 hours at 37ºC. Fluorescence was measured using the EnVision2104

(Per etry using Microsoft Office Excel software. IC_{50} values of compounds were determined by plotting % of inhibition against the Log10 compound test concentration using a four-parametric sigmoidal curve fit with a variable slope in GraphPad Prism version 5.3 for Windows (GraphPad Software, San Diego, CA).

2.4. MDCKII-MDR1 permeability assay

MDCKII-hMDR1 cells were obtained from Solvo Biotechnology, Hungary. DMEM, Fetal bovine serum, Glutamax-100, Antibiotic/Antimycotic, DMSO, Dulbecco's phosphate buffer saline, MEM Non-essential amino acids were purchased from Sigma (St. Louis, MO, USA).
Bi-directional permeability and P-glycoprotein substrate assessment were investigated in Madin-Darby canine epithelial cells with over-expressed human MDR1 gene (MDCKII-MDR1), coding for P-glycoprotein. Experimental procedures, as well as cell culture conditions, were the same as previously described.[32] Briefly, compounds (10 µM, 1% DMSO v/v) in duplicate were incubated at 37°C for 60 min with cell monolayer on 24-well Millicell inserts (Millipore, Burlington, MA, USA) without and with the P-glycoprotein inhibitor Elacridar (2 µM, International Laboratory, USA). Inhibition of P-glycoprotein was verified by amprenavir (Moravek Biochemicals Inc, Brea, CA, USA) and monolayer integrity by Lucifer yellow (Sigma, St. Louis, MO, USA). Compound concentrations were measured by LC-MS/MS and Lucifer yellow was measured on an Infinite F500 (Tecan, Männedorf, CH) using excitation of 485 nm and emission of 530 nm.

2.5. Metabolic stability

Mouse liver microsomes were obtained from Corning Life Sciences (Corning, USA). DMSO, nicotinamide adenine dinucleotide phosphate (NADP), glucose-6-phosphate, glucose-6-phosphate dehydrogenase, magnesium chloride, propranolol, caffeine, diclofenac, phosphate buffer saline (PBS) were purchased from Sigma (St. Louis, MO, USA). Acetonitrile (ACN) and methanol (MeOH) were obtained from Merck (Darmstadt, Germany). Testosterone was purchased from Steraloids (Newport, RI, USA).

Metabolic stability was assessed in mouse liver microsomes. Compounds (final concentration of 1 µM, 0.03% DMSO v/v) were incubated in duplicate in phosphate buffer (50 mM, pH 7.4) at 37°C together with mouse liver microsomes in the absence and presence of the NADPH cofactor (0.5 mM nicotinamide adenine dinucleotide phosphate, 5 mM glucose-6-phosphate, 1.5 U/mL glucose-6-phosphate dehydrogenase and 0.5 mM magnesium chloride). Incubation and sampling was performed on a Freedom EVO 200 (Tecan, Männedorf, CH) at 0.3, 10, 20, 30, 45 and 60 min. The reaction was quenched using 3 volumes of a mixture of ACN/MeOH (2:1) containing internal standard (diclofenac), centrifuged and supernatants were analyzed using LC-MS/MS.
Metabolic activity of microsomes was verified by simultaneous analysis of several controls including testosterone, propranolol and caffeine. The *in vitro* half-life ($t_{1/2}$) was calculated using GraphPad Prism non-linear regression of % parent compound remaining versus time. *In vitro* clearance, expressed as µl/min/mg, was estimated from the *in vitro* half-life ($t_{1/2}$), and normalized for the protein amount in the incubation mixture and assuming 52.5 mg of protein per gram of liver.

2.6. LC-MS/MS analysis

coupled to liquid chromatography. Samples were analysed on a Sciex API4000 Triple Quadrupole Mass Spectrometer (Sciex, Division of MDS Inc., Toronto, Canada) coupled to a Shimadzu Nexera X2 UHPLC frontend (Kyto, Japan). Samples were injected onto a UHPLC column (HALO2 C18, 2.1x20 mm, 2 µm or Luna Omega 1.6 µm Polar C18 100A, 30x2.1 mm) and eluted with a gradient at 50°C. The mobile phase was composed of acetonitrile/water mixture (9/1, with 0.1 % formic acid) and 0.1 % formic acid in deionized water. The flow rate was 0.7 mL/min and under gradient conditions, leading to a total run time of 1.5–2 min. Positive ion mode with turbo spray, an ion source temperature of 550°C and a dwell time of 150 ms were utilized for mass spectrometric detection. Quantitation was performed using multiple reaction monitoring (MRM) at the specific transitions for each compound.

2.7. Computational methods

Known KDM4C inhibitors were retrieved from the Chembl data base.[33] Field-based alignment of representative structures has been performed by the Forge software[34] from the Cresset set of tools. Activity atlas[34] was subsequently used to build up the qualitative generalized pharmacophoric model.

Available crystal structures of protein KDM4C and co-crystalized KDM4C protein with various inhibitors were downloaded from the Protein data bank.[35] Representative ligands from the 2XML, 5FJH and 5FJK X-ray structure were used. The ligand docking studies were carried out using Glide docking protocol[36-37] within Schroedinger software suite[38] with and without extra precision (SP, XP). Docking was performed using metal-ligand constrains and octahedral coordination. Binding poses were refined and binding energies estimated using MM-GBSA[39-40] protocol and OPLS3 force-field with flexible residues distance being 6 Å.
Applicability of MMGBSA and QM/MM methods for this class of enzymes was investigated on KDM4A as a case study. Seven KDM4A inhibitors were selected for which activities as well as co-crystal structures were publicly available (5F2S, 5F2W, 5F5I, 5F32, 5F3I, 5F3E, 5F39).[41]

Quantum Mechanics / Molecular Mechanics (QM/MM) calculations were done with QSite within the Schroedinger software.[38] KDM4A complexes were treated with the Zn (II) and Fe (II) in the metal complexes, Zn being in the single spin state and Fe(II) was investigated in the both singlet and quintet spin states. KDM4C complexes were investigated with the Ni(II) in the triplet state. QM part of the metal complex was treated with B3LYP-D3 functional and 6-31+(2d,p) basis set[42-46] for H,C,O and N atoms and lav3p++(2d,p) basis set for metal ions.[47] MM part was treated with OPLS_2005 force field.[48] The NBO analysis[49] has been done on the optimized geometries. The second order perturbation theory analysis of the Fock matrix in the NBO basis was used to estimate strength of metal ligand donor-acceptor interactions.
Electronic structure and orbital levels were calculated from the optimized geometries at the M06-2x/6-31G(2d,p)+ level. M06-2x functional was used as it was previously shown that it reproduces well ionization energies and electron affinities[50-52]

3. Results and discussion

Compounds for biological evaluation were synthesized in 3 campaigns as described in section 2.1. In the first campaign linear

mol for bi-cyclic pairs based on toxoflavin scaffold (**4a-4k**). In the third campaign a scaffold hopping exercise was done in order to directly modify bi-cyclic toxoflavin scaffold (**Table 1b**, compounds **5a-5c)**.

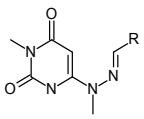

3a-3m

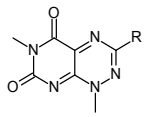

4a-4m

Compound	R	Compound	R
3a, 4a		**3h**	
3b, 4b	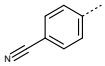	**3i**	
3c, 4c		**3j, 4j**	
3d, 4d	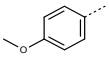	**3k, 4k**	
3e, 4e		**3l, 4l**	
3f, 4f	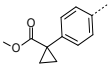	**3m, 4m**	
3g, 4g			

Table 1a. Synthesized compounds**3a-3m** and **4a-4m**.

Compound		
5a	**5b**	**5c**
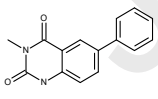	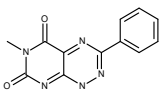	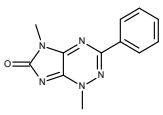

Table 1b. Synthesized compounds**5a-5c**.

3.1. Calibrating computational workflow – KDM4A case study

A recently published set of highly homologous KDM4A protein co-crystal complexes has been used in order to explore applicability of Glide docking protocol, as well as MMGBSA and for KDM4 class of proteins. As the similarity of the catalytic domains of KDM4A and KDM4C is 84%, we assumed that results for KDM4A inhibitors will be transferable to KDM4C inhibitors as well.

Modelling of the metalloenzymes and metal-ligand interactions is highly challenging due to the inadequacies of the force-field to properly account for the coordination bonds and the need to treat the system, or at least the part of the system by quantum-chemical methods.[53-55] Furthermore, an optimal choice of the QM method used in the QM/MM approach is also important in order to obtain high-quality data.[39-41] Current DFT functionals are in general improvements over HF (Hartree-Fock), LDA (local density) and even MP2 calculations, however these improvements are not systematic and often good agreement with experimental data has to be tested empirically for different systems of interest.[56-57] It has been repeatedly reported that B3LYP-D3 functional is the optimal choice for the exploration of metalloenzyme-ligand complexes[53-54, 58-59] and it has been used throughout this study.

In this study, the QM part was composed from the metal ion first coordination sphere including crystal water molecules, His278, triade His190, Thr191, Glu192 and the ligand molecule.

X-ray structures were used as a starting point for the MMGBSA and QM/MM optimizations and the interaction energies were calculated as a difference between energies of a complex and energies of a free ligand and the protein. Since QM/MM optimization calculations are time-demanding, especially in the case of slow convergent calculations for flat potential energy surfaces and higher spin states, single point QM/MM calculations have also been performed on both MMGBSA and x-ray structures to investigate applicability of computationally cheaper workflow. Predicting experimental binding energies or inhibitor potential of ligands is a highly challenging task. It has been shown previously that experimental activity data can be estimated reasonably well as a linear combination of QM/MM interaction energies and desolvation-characterizing changes in the solvent-accessible surface areas.[55] Authors have used linear interaction energy approximation and calculated binding free energies as a linear combination of the differences Δ in the van der Waals energies, electrostatic energies and the solvent accessible surface areas (SASA) obtained from molecular dynamics (MD) or Monte Carlo simulations approximatively describing desolvation penalties and hydrophobic effects as a result of amount of SASA buried upon complexation:

$$\Delta G_b = \alpha \times \Delta\langle E_{vdW}\rangle + \beta \times \Delta\langle E_{el}\rangle + \gamma \times \Delta\langle SASA\rangle + \kappa$$

A similar method for the treatment of hydration of more complex molecules required the use H-bond donor and acceptor counts.[60] In order to explore if further simplifications could be used, while still obtaining at least semi-quantitative agreement with the experimental activities, we assumed that the protein desolvation energies are similar for all examined complexes and will be accounted for by regression coefficients. Conformational changes of the ligands upon binding are also assumed to be small due to the rigidity of the compounds and ΔSASA was approximated with the SASA for the free compound in the water. QM/MM energies were combined linearly with the desolvation contribution approximated by different descriptors describing ligand solvent-accessible

surf one (Hydrophobic component of the SASA), FISA (Hydrophilic component of the SASA), PISA (π component of the SASA) HBA, HBD, dipole, volume and globularity.[61] Experimental activities, expressed as pIC_{50} values, were correlated with QM/MM energies and QikProp [62] descriptors described above using PLS (partial-least square method).[63] Good correlation has been obtained for the set of 7 KDM4A-ligand complexes as shown on **Figure 2**. Values of descriptors used in the model development are given in the **Table S1** (Supplementary data). Correlation of the QM/MM interaction energies with pIC_{50} values were R^2=0.73 and 0.71 for the SP and fully optimised geometries.

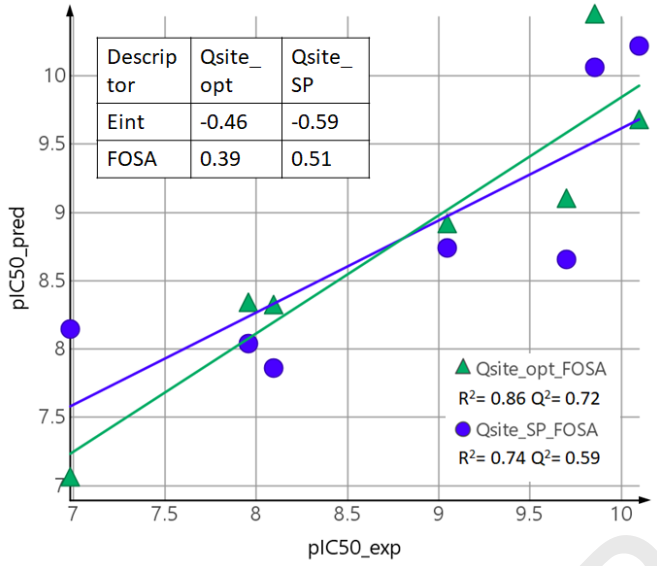

Figure 2. Correlation between experimental and predicted pIC_{50} values for a set of KDM4A inhibitors.

The strength of the ligand coordination to the metal ion was additionally quantified in terms of the second order perturbation theory analysis of the Fock matrix in the NBO basis. Delocalization of the N(4) lone-pair electron density into the unfilled valence-shell nonbonding orbitals of the metal ion ranges from 44-64 kcal/mol for 5F2S, 5F2W, 5F51 and 5F32 ligands as shown in **Table S1.**

Results for the KDM4A case study encouraged us to proceed with the QM/MM calculations of the interaction energies for the designed set of potential KDM4C inhibitors based on the toxoflavin scaffold.

3.2. Key features of KDM4C active site

KDM4C is a metalloprotein containing Fe(II) ion which is substituted with Ni(II) in co-crystallization studies.[64] It belongs to alpha-ketoglutarate-dependent hydroxylase superfamily and requires α-ketoglutarate as a cofactor to exert its biological activity. Three x-ray structures were publicly available: 2XLM, 5FJK and 5FJH.

Ni(II) ion has an octahedral coordination filled with His 190, His 278, Glu192 from the protein and one or two water molecules depending if the inhibitor is monodentate of bidentate ligand (**Figure 3**). α-ketoglutarate acts as a bidentate ligand as well as isonicotinic acid derivative from the 5FJH structure, while coordination position and therefore contains two water molecules in the metal coordination sphere. Additional H-bond interactions are formed with the side chains on the opposite side of the binding pocket: Tyr134, Lys208 and Asn200 as shown on the **Figure 5.** Lys243 is displaced and the salt bridge between Lys243 and Asp137 is broken in the 5FJK structure, in comparison with 5FJH and 2XML structures, keeping the entrance channel open. Also, Tyr 134 is displaced to the bottom of the binding pocket enabling ligand to position across the binding site, form pi-pi stacking with the phenyl ring of Tyr134 and H-bonding interactions with Lys208. Hydroxy groups of Ser198 and Ser290 are assumed to be differently oriented due to the H-bond network with coordinated water molecules. Available x-ray structures therefore demonstrate different binding coordinations and significant protein conformational changes due to induced fit of diverse inhibitor chemotypes.

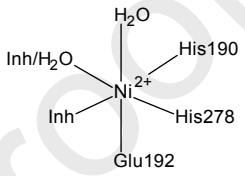

Figure 3. Coordination of Ni^{2+} ion forming octahedral coordination.

3.3. Field-based analysis of known KDM4C inhibitors

Known KDM4C inhibitors were retrieved from the Chembl database.[33] Based on the activity range and structural diversity, 40 compounds were selected for field-based alignment with ligands from the 5FJH and 5FJK X-ray structures. Subsequently, a field-based pharmacophoric model was built using the Activity atlas tool from Cresset suite of software. These results were used together with the SBDD information in order to design a focused library based on the toxoflavin scaffold. As shown in **Figure 4.,** a major electrostatic contribution for the KDM4C inhibitors are negative electrostatic fields from the nitrogen lone pairs contributing to the metal-ion coordination, as well as electron rich groups (carboxylic acid in the case of 5FJH ligand) that form a strong H-bond network with Tyr134, Lys208 and Asn200. This was also seen from the available x-ray structures. In addition, the average shape of actives was calculated. The toxoflavin scaffold was aligned with the reference 5FJH ligand to explore possible binding modes and further modifications. Field-based analysis showed that toxoflavin fits well within the generalized pharmacophore model and that position C3 is suitable for further diversification. Compound **4a** was used as representative molecule to explore if the aromatic ring could be accommodated within the average shape of actives. It was clear that the alignment is good, however, both monodentate and bidentate binding will have to compromise direct metal coordination and fit into the region populated by investigated active compounds. Therefore, induced fit and the side-chain displacement of some amino-acids in the binding pocket could be expected in order to accommodate the designed compounds, as already observed in the 5FJK structure as well as some of the available KDM4A co-crystal structures.

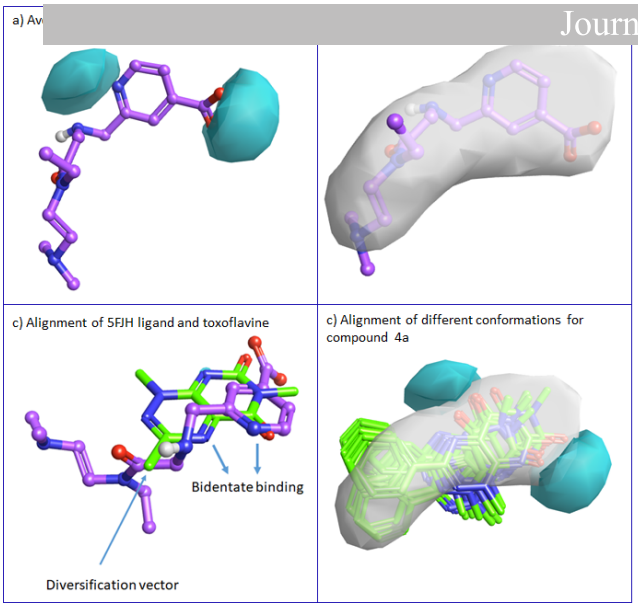

Figure 4. Field-based pharmacophoric features of KDM4C inhibitors: a) average negative field of actives, b) average shape of actives, c) alignment of 5FJH ligand with toxoflavin, d) alignment of different conformations for compound **4a**.

3.4. Investigation of KDM4C interactions with toxoflavin derivatives

Docking studies. Potential binding modes for the proposed toxoflavin-based focused library were investigated by docking into both, 5FJH/2XML and 5FJK X-ray structures. In the case of 5FJH structure, bidentate and monodentate binding modes were explored. For the 5FJK structure, only the monodentate binding mode was investigated with two coordinated water molecules. To enable bidentate binding into 5FJH structure, Lys243 side-chain was displaced as in the 2XML and 5FJK structure. Water orientations and possible H-bonded networks were optimized using a refinement procedure from the protein preparation wizard and interactive H-bond optimizer. The SP docking protocol with constrains defined as metal-ligand interaction and octahedral coordination gave the best results.
Proposed docking pose for the toxoflavin itself into 2XML is shown on **Figure 5a** confirming findings from the ligand-based analysis that diversification vector could be placed at the C3 atom on the toxoflavin scaffold. Docking of compound **4a** resulted in bidentate binding within the 5FJH and monodentate binding into 5FJK structure using SP accuracy level as shown in the **Figure 5b. Figure 5b** also illustrates different binding modes and different sub pockets filled with ligands from currently available X-ray structures.

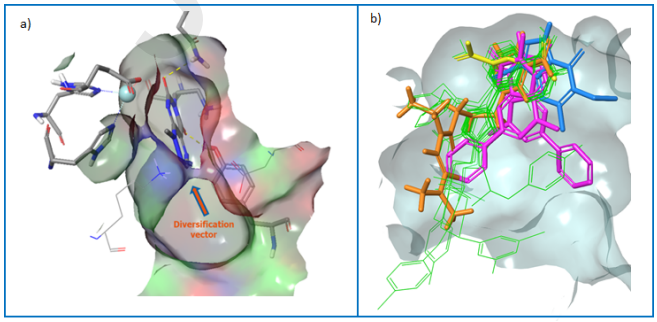

Figure 5. a) Proposed toxoflavin binding mode in the active site of KDM4C enzyme (PDB:5FJH used). b) Alignment of 2XML ligand-yellow; KDM4A inhibitors-green; 5FJH ligand-orange; 5FJK ligand-magenta.

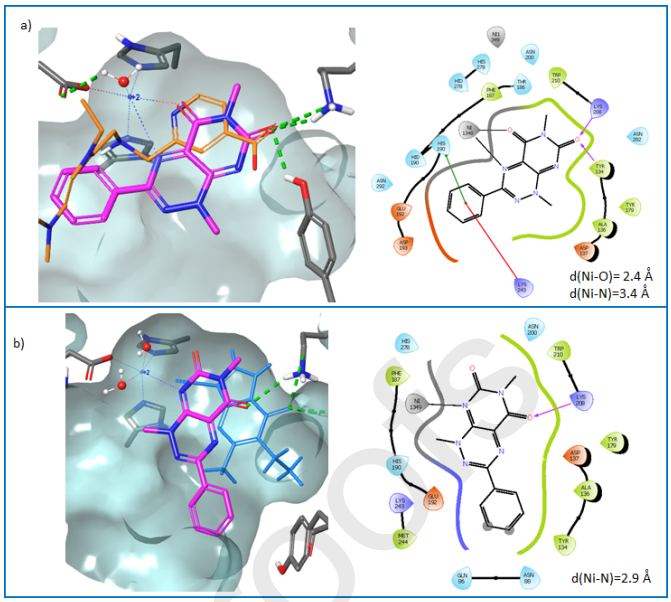

Figure 6. a) MMGBSA optimized geometry of compound **4a** aligned with 5FJH ligand and corresponding 2D diagram. b) MMGBSA optimized geometry of compound **4a** aligned with 5FJK ligand and corresponding 2D diagram

MMGBSA and QM/MM studies. Complexes obtained by docking were further minimized using MMGBSA and used in the QM/MM calculations where QM part was kept fixed and MM part was minimized. Final geometries are shown on **Figure 6**; bidentate binding mode of compound **4a** is shown on **Figure 6a** and monodentate on **Figure 6b**. In both cases, major interactions with the protein are formed by metal coordination of 8-N and 7-CO oxygen and H-bonds between 5-CO oxygen and Lys208 and Tyr134. NBO analysis showed that delocalization of the nitrogen and oxygen lone-pair electron density into the unfilled valence-shell nonbonding orbitals of the metal ion were in the range of KDM4A complexes; 22 and 45 kcal/mol; while electron delocalization was much stronger for the 5FJH and 5FJK ligands; 162 and 138 kcal/mol, respectively.
Correlation between experimentally determined inhibitory activities with QM/MM energies calculated for the both monodentate and bidentate binding is shown in section 3.5.1.

3.5 *In vitro* biological profiling

3.5.1. Inhibition activity against KDM4C enzyme. Most of the linear compounds displayed inhibition of 40% or less at concentration of 10 µM. Compounds **3c**, **3d** and **3l** showed inhibition in range 40-70%. Among the best linear compounds were **3a** and **3m** with an inhibition over 70%. All cyclic molecules showed inhibition of 100%, and therefore they were tested in a secondary screening assay to calculate the IC_{50}. Results are presented in **Table 3**. All cyclic molecules displayed inhibition activity in the nanomolar range. Compared to the published activity of toxoflavin (IC_{50} = 541 nM, CHEMBL578512), compounds **4a-4m** showed improved activity, probably due to the additional interactions of substituted phenyl ring with the protein. However, binding efficiency of toxoflavin derivatives were not improved over the toxoflavin scaffold (**Table S2**), pointing to non-specific hydrophobic interactions of additional phenyl ring and inability to form perfect octahedral coordination to the metal ion.

In o
toxoflavin and introduce additional chemical diversity, scaffold hopping exercise was performed. Several structural modifications have been made (**Table 1b**) with intention to reduce redox potential and retain good activity. Although a drop in IC_{50} values in the biochemical assay to the micromolar range was observed (**Table 3**), both **5b** and **5c** could be considered as a novel starting points for further medicinal chemistry efforts.

Table 3. Inhibition activity on KDM4C, passive permeability, P-gp substrate indication, microsomal stability (Clint), and influence on cell proliferation on HepG2 and A549 cell-lines for tested compounds; toxoflavin (IC_{50} = 541 nM, CHEMBL578512).

Cpd	KDM4C IC_{50} [nM]	Passive permeability(A2B) Papp [x10-6 cm/sec]	P-gp substrate	Clint [µl/min/mg]	HepG2 IC_{50} [uM]	A549 IC50 (µM)
4a	130	34.7	-	<12.5	0.87	1.1
4b	11	26.8	-	<12.5	0.80	1.9
4c	242	13.2	-	<12.5	1.1	5.8
4d	8	34.5	-	<12.5	0.80	1.1
4e	42	0.8	-	<12.5	5.6	>30
4f	NA	24.9	+	<12.5	1.2	1.3
4g	29	25.3	-	<12.5	5.1	>30
4j	19	13.4	-	11.6	1.8	4.3
4k	NA	1.1	-	71850	4.5	8.8
4l	16	18.0	-	<12.5	2.1	5.7
4m	81	30.6	-	<12.5	0.82	1.6
5a	>10000	27.3	-	229.1	>25	>30
5b	7626	35.5	-	<12.5	>25	>30
5c	12650	40.6	-	13.1	>25	>30
Toxoflavin	541[33]	16.0	-	<12.5	4.5	0.022

Experimental activities expressed as pIC_{50} values were correlated, with QM/MM energies calculated for the both monodentate and bidentate binding and QikProp descriptors described, using partial-least square method (as described in section 3.1. for KDM4A case study). Results are shown in **Figure 7** and **Table S2**. A statistical model similar to that of KDM4A data set has been developed with ΔEint, dipole and FOSA (hydrophobic part of solvent accessible surface area) as descriptors. The developed model can be further used to estimate activity of new potential KDM4C inhibitors structurally similar to toxoflavin scaffold.

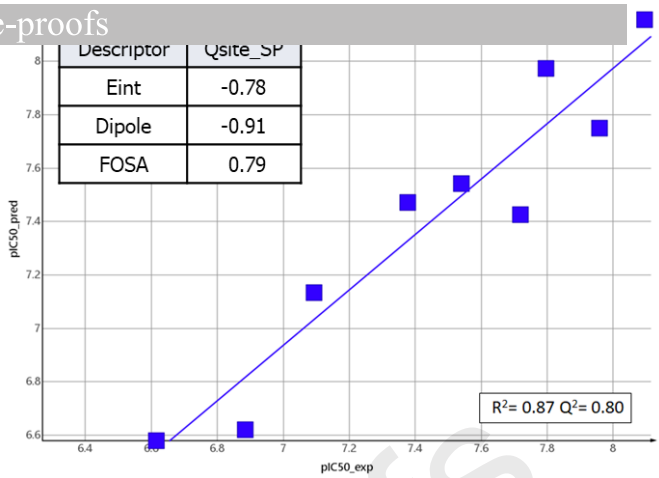

Figure 7. Correlation between experimental and predicted pIC_{50} values for a set of KDM4C inhibitors based on toxoflavin scaffold.

Results from *in vitro* ADME profiling including MDCKII-MDR1 permeability and microsomal metabolic stability are summarized in the **Table 3**.

3.5.2. MDCKII-MDR1 permeability assay. The majority of tested compounds showed a high passive permeability, with Papp(A2B) values in the presence of P-gp inhibitor ranging from 10.8 to 34,5x10^{-6} cm/s. Two compounds were classified as low permeable, **4e** and **4k** with permeability values <2 x10^{-6} cm/s. According to the literature[65-66] the permeability of the majority of compounds tested was not influenced by P-glycoprotein, i.e., efflux ratio (Papp(BA)/Papp(AB)) was lower than 2 and/or in the presence of inhibitor was not decreased by more than 50 % when compared with efflux ratio without P-gp inhibitor. Only compound **4f** was classified as possible P-gp substrate.

3.5.3. Metabolic stability. Incubation with mouse liver microsomes showed that all tested compounds were stable molecules with clearance values below 12.5 µl/min/mg protein, except for **5a** which showed high clearance profile. In addition, compound **4k** showed matrix instability and therefore the Clint value could not be obtained.

3.6. Redox potential of toxoflavin derivatives

In order to better understand the electronic structure of prepared toxoflavin derivatives and investigate possible link with measured influence on cell viability, their redox potentials have been calculated.

As already published for flavin scaffold, redox potential can be modulated by substituents with different properties.[67] Toxoflavin as a natural product is known to possess redox properties that result in the reduction of a cell viability. The mechanism of reaction is similar to those of flavins and it was shown to proceed over the following mechanism:

$$NADH + Toxoflavin \rightarrow NAD^{+} + Toxoflavin\text{-}H_2$$

$$Toxoflavin\text{-}H_2 + O_2 \rightarrow Toxoflavin + H_2O_2$$

where the hydrogen peroxide as a toxic species is produced.[68] Toxoflavin derivatives investigated in this paper are planar in the oxidized form and bent to ±142° in the reduced form due to the nitrogen pyramidalization as already demonstrated for flavin derivatives.[69-70]

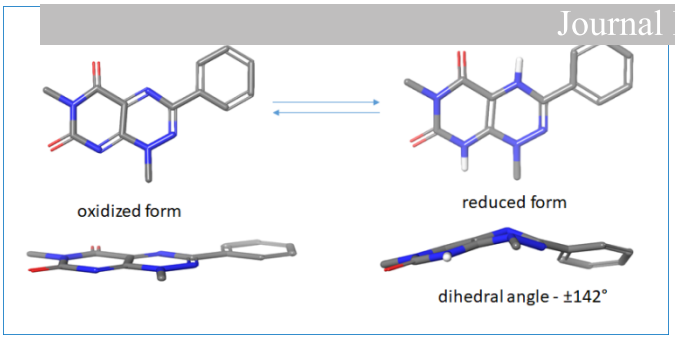

Figure 8. Planar and butterfly bent geometries of Ph substituted toxoflavin derivative (3a) in oxidized and reduced form.

Influence on the redox potential by R1 substitutions of phenyl scaffold was investigated in terms of the changes of the LUMO energy levels for the oxidized form and HOMO energy levels of the reduced form as shown on **Figure 9**. DFT theory at the M06-2x/6-31(2d,p)+ level was used for the geometry optimisation and calculation of the electronic properties as described in the method section.

A decrease of the redox potential is expected to be a net effect of the destabilization of the LUMO orbital of the oxidized form in comparison to the toxoflavin (as it will require more energy to fill in additional electrons) and stabilization of the HOMO orbital of the reduced form (as it will require more energy to extract the electrons) as shown on **Figure 9**.

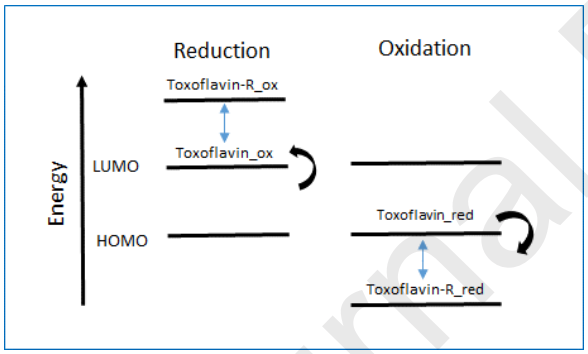

Figure 9. Schematic presentation of the desired influence of the substitution on the toxoflavin scaffold in order to decrease the redox potential.

Indeed, LUMO orbitals of investigated derivatives in the oxidised form are destabilised for prepared analogues in comparison to toxoflavin. This indicates lower reduction affinity. However, negative energy values indicate that reduction is still an energy-favoured process for investigated toxoflavin derivatives.

Comparing significantly higher orbital energies of acyclic compounds, where the diazaallene system is not existing, with cyclic Ph-substituted toxoflavin derivatives, the question still remains if this LUMO destabilisation is significant enough to decrease redox potential and potential non-specific toxicity of Ph-substituted compounds. However, the HOMO orbitals of reduced forms are also destabilised by substitutions making them more prone to the oxidation, except in case of compounds **3b** and **3e**.

ses, reduction as a first step is expected to be slower than for the toxoflavin scaffold, similarly to early work on flavines by Hall *et. al*.

As expected, HOMO orbital of reduced form resembles the LUMO orbital of the oxidized form. It is π* orbital mostly localized on the diazaallene system and lone pair of the neighbouring nitrogen atom. Both, HOMO orbital of the oxidised form and LUMO of the reduced form also have contributions from the electron density distribution on the phenyl substituent.

It is also interesting to note that the lone-pair of the N8 from the diazaallene system populates HOMO of the oxidised form while the other N4 lone pair is part of the LUMO orbital. This might explain preferential coordination of N8 to the metal ion that we found from the docking and QM/MM.

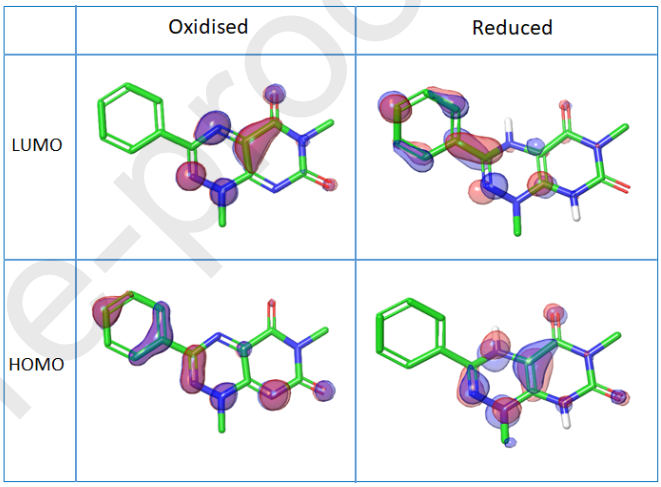

Figure10. Frontier orbitals for the oxidized and reduced forms of compound **3a**.

Predicted reduction and oxidation potentials of toxoflavin derivatives were compared with measured and calculated redox potentials for polycyclic aromatic hydrocarbons as shown on **Figure 11**.[71-72] Predicted redox potentials were calculated from the frontier orbital energies using regression equation for PAHs. Reduction potentials of investigated toxoflavin derivatives are in the range of the potentials measured and calculated for PAHs, while oxidation potentials of reduced forms are higher than those of PAHs.

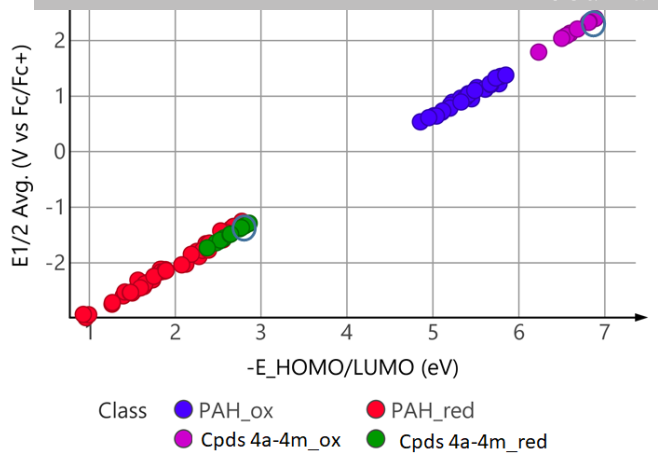

Figure 11. Plot of computed HOMO/LUMO energies (eV) vs. experimental E1/2 avg. Circled are values for toxoflavin as a reference.

3.7. Influence on HepG2 and A549 cell line proliferation

Proliferation of HepG2 and A549 cell lines after 24 and 72 hours of incubation time with tested compounds was investigated. Results are shown in **Table 3**. Compounds **4a-4m** are found to influence the cell proliferation on both cell lines with IC_{50} in low µM range. Exceptions are compounds **4e** and **4g** that showed no influence on proliferation of A549 cells. Compounds **5a-5c** showed no influence on cell proliferation on both cell-lines. These results are in line with measured activity on KDM4C enzyme. However, influence on the cell proliferation is expected to be a combination of target based activity on KDM4C (and probably other close analogues from the KDM4 class of enzymes) and non-specific toxicity due to the oxido-reductive potential of the toxoflavin scaffold. Since results on the HepG2 cell-line are comparable with those for A549 cell-line, despite significantly longer incubation time in case of A549 cell-line, this indicates that major factor influencing the cell-line proliferation could be specific, target based activity on KDM4C enzyme. Such conclusion is further supported by results we obtained for toxoflavin itself, where IC_{50} on A549 cell-line is two orders of magnitude lower that on HepG2 cell-line, and also one order of magnitude lower than its binding activity on KDM4C.

Correlation between inhibitory KDM4C enzyme activity and influence on the cell proliferation is graphically shown on **Figure 12a** and **b**. In order to further explore major factors influencing cellular proliferation, partial least square (PLS) analysis has been performed to build up mechanistic models. Beside KDM4C inhibitory activity, several structural parameters were calculated; clogP, total polar surface area (TPSA), number of hydrogen bond donors and acceptors (HBD, HBA). In addition, experimental permeability (Papp (AB)) and calculated HOMO/LUMO orbital shifts were used as independent variables. PLS models for the influence on cell-proliferation for HepG2 and A549 cell-lines are given on **Figure 12c** and **d**. Experimental values, calculated parameters and predicted IC_{50} values are listed in **Table S3**. It is interesting to note that HepG2 cell proliferation can be predicted from specific KDM4C inhibitory activity, permeability into cells and calculated logP values. Cell proliferation on A549 cells is

bital
shifts of oxidised form for investigated compounds. This is in line with the longer time scale in the experimental setup for A549 cell lines where unspecific toxic effects could have more influence on the measured IC_{50} values. It is important to note that for A549 cell proliferation model toxoflavin was excluded since none of envisaged independent variables could not explain significant difference between cell proliferation on HepG2 and A549 cell-lines. As stated previously, this could be indication that non-specific toxicity of toxoflavin due to its redox potential is reduced for the investigated toxoflavin derivatives.

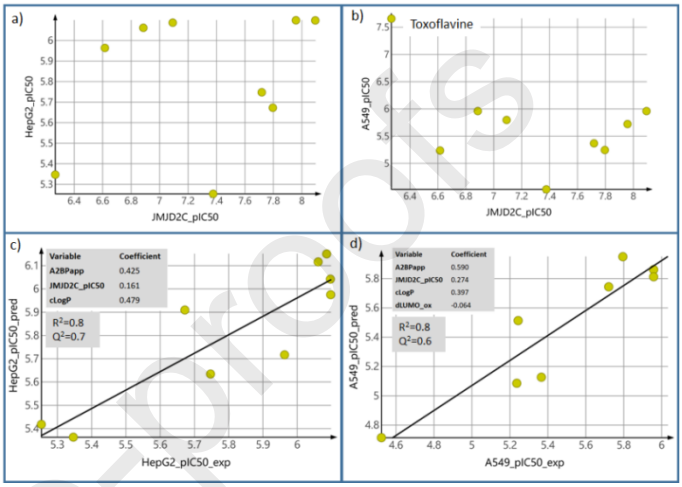

Figure 12. Inhibitory KDM4C enzyme activity vs. influence on the cell proliferation for a) HepG2 and b) A549 cell-lines. Experimental vs. predicted pIC_{50} values for c) HepG2 and d) A549 cell lines.

4. Conclusions

Focused library of non-carboxylate inhibitors of the KDM4C histone lysine demethylase based on toxoflavin scaffold has been designed, synthesized and profiled in biochemical and cell-based assays. In order to minimize redox liability of toxoflavin, substituents with different electronic properties were introduced.

Several compounds were identified as potent inhibitors of KDM4C with activity in low nM range in the target-specific biochemical assay and in the µM range in the cell-based assay. Active compounds possess improved *in vitro* ADME properties with good passive cellular permeability and metabolic stability.

Structural interactions of prepared inhibitors with the active site of KDM4C have been analysed with the optimized docking protocol, energetics of the interactions was predicted by advanced QM/MM hybrid approach and redox potential was calculated by hybrid DFT methods. Statistical analysis of collected data has been performed in order to get mechanistic insight into the major factors influencing cellular activity of investigated compounds.

distinguish activity on the KDM4C enzyme, redox liability and non-specific influence on cell viability as well as possible interactions with other targets still needs to be performed. Nevertheless, interesting hit molecules with strong KDM4C potency and good ADME profile are identified as a good starting point for further optimization and characterization.

Conflicts of interest

There are no conflicts to declare.

Notes and references

1. Zinchenko, A.; Berezhnoy, N. V.; Wang, S.; Rosencrans, W. M.; Korolev, N.; van der Maarel, J. R. C.; Nordenskiold, L., Single-molecule compaction of megabase-long chromatin molecules by multivalent cations. *Nucleic Acids Res* **2018,** *46* (2), 635-649.
2. Bannister, A. J.; Kouzarides, T., Regulation of chromatin by histone modifications. *Cell Res* **2011,** *21* (3), 381-95.
3. Martin, C.; Zhang, Y., The diverse functions of histone lysine methylation. *Nat Rev Mol Cell Biol* **2005,** *6* (11), 838-49.
4. Hublitz, P.; Albert, M.; Peters, A. H., Mechanisms of transcriptional repression by histone lysine methylation. *Int J Dev Biol* **2009,** *53* (2-3), 335-54.
5. Cloos, P. A.; Christensen, J.; Agger, K.; Helin, K., Erasing the methyl mark: histone demethylases at the center of cellular differentiation and disease. *Genes Dev* **2008,** *22* (9), 1115-40.
6. Bonasio, R.; Tu, S.; Reinberg, D., Molecular signals of epigenetic states. *Science* **2010,** *330* (6004), 612-6.
7. Pasini, D.; Bracken, A.; Agger, K.; Christensen, J.; Hansen, K.; Cloos, P.; Helin, K., Regulation of Stem Cell Differentiation by Histone Methyltransferases and Demethylases. *Cold Spring Harb Symp Quant Biol.* **2008**; 73, 253-63.
8. Berry, W. L.; Janknecht, R., KDM4/JMJD2 histone demethylases: epigenetic regulators in cancer cells. *Cancer Res* **2013,** *73* (10), 2936-42.
9. Agger, K.; Christensen, J.; Cloos, P. A.; Helin, K., The emerging functions of histone demethylases. *Curr Opin Genet Dev* **2008,** *18* (2), 159-68.
10. Hake, S. B.; Xiao, A.; Allis, C. D., Linking the epigenetic 'language' of covalent histone modifications to cancer. *Br J Cancer* **2004,** *90* (4), 761-9.
11. Mallette, Frédérick A.; Richard, S., JMJD2A Promotes Cellular Transformation by Blocking Cellular Senescence through Transcriptional Repression of the Tumor Suppressor CHD5. *Cell Reports* **2012,** *2* (5), 1233-1243.
12. Labbe, R. M.; Holowatyj, A.; Yang, Z. Q., Histone lysine demethylase (KDM) subfamily 4: structures, functions and therapeutic potential. *Am J Transl Res* **2013,** *6* (1), 1-15.
13. Young, L. C.; Hendzel, M. J., The oncogenic potential of Jumonji D2 (JMJD2/KDM4) histone demethylase overexpression. *Biochem Cell Biol* **2013,** *91* (6), 369-77.
14. Ye, Q.; Holowatyj, A.; Wu, J.; Liu, H.; Zhang, L.; Suzuki, T.; Yang, Z.-Q., Genetic alterations of KDM4 subfamily cancer. *Am J Cancer Res* **2015,** *5* (4), 1519-1530.
15. Kawamura, A.; Münzel, M.; Kojima, T.; Yapp, C.; Bhushan, B.; Goto, Y.; Tumber, A.; Katoh, T.; King, O. N. F.; Passioura, T.; Walport, L. J.; Hatch, S. B.; Madden, S.; Müller, S.; Brennan, P. E.; Chowdhury, R.; Hopkinson, R. J.; Suga, H.; Schofield, C. J., Highly selective inhibition of histone demethylases by de novo macrocyclic peptides. *Nature Commun* **2017,** *8*, 14773.
16. Lin, H.; Li, Q.; Li, Q.; Zhu, J.; Gu, K.; Jiang, X.; Hu, Q.; Feng, F.; Qu, W.; Chen, Y.; Sun, H., Small molecule KDM4s inhibitors as anti-cancer agents. *J Enzyme Inhibit Med Chem* **2018,** *33*, 777-793.
17. Zhang, C.; Wang, Z.; Ji, Q.; Li, Q., Histone demethylase JMJD2C: epigenetic regulators in tumors. *Oncotarget* **2017,** *8* (53), 91723-91733.
18. Garcia, J.; Lizcano, F., KDM4C Activity Modulates Cell Proliferation and Chromosome Segregation in Triple-Negative Breast Cancer. *Breast Cancer (Auckl)* **2016,** *10*, 169-175.
19. Thinnes, C. C.; England, K. S.; Kawamura, A.; Chowdhury, R.; Schofield, C. J.; Hopkinson, R. J., Targeting histone lysine demethylases - progress, challenges, and the future. *Biochim Biophys Acta* **2014,** *1839* (12), 1416-1432.
20. Westaway, S. M.; Preston, A. G.; Barker, M. D.; Brown, F.; Brown, J. A.; Campbell, M.; Chung, C. W.; Diallo, H.; Douault, C.; Drewes, G.; Eagle, R.; Gordon, L.; Haslam, C.; Hayhow, T. G.; Humphreys, P. G.; Joberty, G.; Katso, R.; Kruidenier, L.; Leveridge, M.; Liddle, J.; Mosley, J.; Muelbaier, M.; Randle, R.; Rioja, I.; Rueger, A.; Seal, G. A.; Sheppard, R. J.; Singh, O.; Taylor, J.; Thomas, P.; Thomson, D.; Wilson, D. M.; Lee, K.; Prinjha, R. K., Cell Penetrant Inhibitors of the KDM4 and KDM5 Families of Histone Lysine Demethylases. 1. 3-Amino-4-pyridine Carboxylate Derivatives. *J Med Chem* **2016,** *59* (4), 1357-69.
21. Westaway, S. M.; Preston, A. G. S.; Barker, M. D.; Brown, F.; Brown, J. A.; Campbell, M.; Chung, C.-W.; Drewes, G.; Eagle, R.; Garton, N.; Gordon, L.; Haslam, C.; Hayhow, T. G.; Humphreys, P. G.; Joberty, G.; Katso, R.; Kruidenier, L.; Leveridge, M.; Pemberton, M.; Rioja, I.; Seal, G. A.; Shipley, T.; Singh, O.; Suckling, C. J.; Taylor, J.; Thomas, P.; Wilson, D. M.; Lee, K.; Prinjha, R. K., Cell penetrant inhibitors of the KDM4 and KDM5 families of histone lysine demethylases. 2. Pyrido[3,4-d]pyrimidin-4(3H)-one derivatives. *J Med Chem* **2016,** *59* (4), 1370-1387.
22. Franci, G.; Sarno, F.; Nebbioso, A.; Altucci, L., Identification and characterization of PKF118-310 as a KDM4A inhibitor. *Epigenetics* **2017,** *12* (3), 198-205.
23. Davies, M.; Nowotka, M.; Papadatos, G.; Dedman, N.; Gaulton, A.; Atkinson, F.; Bellis, L.; Overington, J. P., ChEMBL web services: streamlining access to drug discovery data and utilities. *Nucleic acids Res* **2015,** *43* (W1), W612-W620.
24. Raoof, A.; Depledge, P.; Hamilton, N. M.; Hamilton, N. S.; Hitchin, J. R.; Hopkins, G. V.; Jordan, A. M.; Maguire, L. A.; McGonagle, A. E.; Mould, D. P.; Rushbrooke, M.; Small, H. F.; Smith, K. M.; Thomson, G. J.; Turlais, F.; Waddell, I. D.; Waszkowycz, B.; Watson, A. J.; Ogilvie, D. J., Toxoflavins and Deazaflavins as the First Reported Selective Small Molecule Inhibitors of Tyrosyl-DNA Phosphodiesterase II. *J Med Chem* **2013,** *56* (16), 6352-6370.
25. Todorovic, N.; Giacomelli, A.; Hassell, J. A.; Frampton, C. S.; Capretta, A., Microwave-assisted synthesis of 3-aryl-pyrimido[5,4-e][1,2,4]triazine-5,7(1H,6H)-dione libraries: derivatives of toxoflavin. *Tetrahedron Lett* **2010,** *51* (46), 6037-6040.

26. Samanta, S.; Kuang, Y.; Ljungman, M.; Neamati, N., Discovery and Mechanistic Elucidation of a Class of Protein Disulfide Isomerase Inhibitors for the Treatment of Glioblastoma. *Chem Med Chem* **2018,** *13* (2), 164-177.
27. Zeller, J.; Turbiak, A. J.; Powelson, I. A.; Lee, S.; Sun, D.; Showalter, H. D. H.; Fearon, E. R., Investigation of 3-aryl-pyrimido[5,4-e][1,2,4]triazine-5,7-diones as small molecule antagonists of β-catenin/TCF transcription. *Bioorg Med Chem Lett* **2013,** *23* (21), 5814-5820.
28. Nagamatsu, T.; Yamasaki, H., General syntheses of 1-alkyltoxoflavin and 8-alkylfervenulin derivatives of biological significance by the regioselective alkylation of reumycin derivatives and the rates of transalkylation from 1-alkyltoxoflavins into nucleophiles. *J Chem Soc, Perkin Trans 1* **2001,** (2), 130-137.
29. Yoneda, F.; Higuchi, M.; Nitta, Y., Synthesis of some 5H-imidazo[4,5-e]-as-triazin-6-(7H)ones (6-azapurin-8-ones). *J Heterocycl Chem* **1980,** *17* (5), 869-871.
30. Whetstine, J. R.; Nottke, A.; Lan, F.; Huarte, M.; Smolikov, S.; Chen, Z.; Spooner, E.; Li, E.; Zhang, G.; Colaiacovo, M.; Shi, Y., Reversal of histone lysine trimethylation by the JMJD2 family of histone demethylases. *Cell* **2006,** *125* (3), 467-81.
31. Mosmann, T., Rapid colorimetric assay for cellular growth and survival: application to proliferation and cytotoxicity assays. *J Immunol Methods* **1983,** *65* (1-2), 55-63.
32. Nožinić, D.; Milić, A.; Mikac, L.; Ralić, J.; Padovan, J.; Antolović, R., Assessment of macrolide transport using PAMPA, Caco-2 and MDCKII-hMDR1 assays. *Croat Chem Acta* **2010,** *83*.
33. Gaulton, A.; Hersey, A.; Nowotka, M.; Bento, A. P.; Chambers, J.; Mendez, D.; Mutowo, P.; Atkinson, F.; Bellis, L. J.; Cibrian-Uhalte, E.; Davies, M.; Dedman, N.; Karlsson, A.; Magarinos, M. P.; Overington, J. P.; Papadatos, G.; Smit, I.; Leach, A. R., The ChEMBL database in 2017. *Nucleic Acids Res* **2017,** *45* (D1), D945-D954.
34. Cheeseright, T.; Mackey, M.; Rose, S.; Vinter, A., Molecular field extrema as descriptors of biological activity: definition and validation. *J Chem Inf Model* **2006,** *46* (2), 665-76.
35. Berman, H. M.; Westbrook, J.; Feng, Z.; Gilliland, G.; Bhat, T. N.; Weissig, H.; Shindyalov, I. N.; Bourne, P. E., The Protein Data Bank. *Nucleic Acids Res* **2000,** *28* (1), 235-42.
36. Friesner, R. A.; Murphy, R. B.; Repasky, M. P.; Frye, L. L.; Greenwood, J. R.; Halgren, T. A.; Sanschagrin, P. C.; Mainz, D. T., Extra precision glide: docking and scoring incorporating a model of hydrophobic enclosure for protein-ligand complexes. *J Med Chem* **2006,** *49* (21), 6177-96.
37. Friesner, R. A.; Banks, J. L.; Murphy, R. B.; Halgren, T. A.; Klicic, J. J.; Mainz, D. T.; Repasky, M. P.; Knoll, E. H.; Shelley, M.; Perry, J. K.; Shaw, D. E.; Francis, P.; Shenkin, P. S., Glide: a new approach for rapid, accurate docking and scoring. 1. Method and assessment of docking accuracy. *J Med Chem* **2004,** *47* (7), 1739-49.
38. Schroedinger *MacroModel, Schroeodinger, LLC*, **2017.**
39. Li, J.; Abel, R.; Zhu, K.; Cao, Y.; Zhao, S.; Friesner, R. A., The VSGB 2.0 model: a next generation energy model for high resolution protein structure modeling. *Proteins* **2011,** *79* (10), 2794-812.
40. Shivakumar, D.; Williams, J.; Wu, Y.; Damm, W.; Shelley, J.; Sherman, W., Prediction of Absolute Solvation Free Energies using Molecular Dynamics Free Energy Perturbation and the OPLS Force Field. *J Chem Theory Comput* **2010,** *6* (5), 1509-1519.
41. Bavetsias, V.; Lanigan, R. M.; Ruda, G. F.; Atrash, B.; McLaughlin, M. G.; Tumber, A.; Mok, N. Y.; Le Bihan, Y. V.; Savitsky, P.; Velupillai, S.; Krojer, T.; England, K. S.; Sejberg, J.; Thai, C.; Donovan, A.; Pal, A.; Scozzafava, G.; Bennett, J. M.; Kawamura, A.; Johansson, C.; Szykowska, A.; Gileadi, C.; Burgess-Brown, N. A.; von Delft, F.; Oppermann, U.; Walters, Z.; Shipley, J.; Raynaud, F. I.; Westaway, S. M.; Prinjha, R. K.; Fedorov, O.; Burke, R.; Schofield, C. J.; Westwood, I. M.; Bountra, C.; Muller, S.; van Montfort, R. L.; Brennan, P. E.; Blagg, J., 8-Substituted Pyrido[3,4-d]pyrimidin-4(3H)-one Derivatives As Potent, Cell Permeable, KDM4 (JMJD2) and KDM5 (JARID1) Histone Lysine Demethylase Inhibitors. *J Med Chem* **2016,** *59* (4), 1388-409.
42. Becke, A. D., Density-functional thermochemistry. III. The role of exact exchange. *J Chem Phys* **1993,** *98* (7), 5648-5652.
43. Lee, C.; Yang, W.; Parr, R. G., Development of the Colle-Salvetti correlation-energy formula into a functional of the electron density. *Phys Rev B* **1988,** *37* (2), 785-789.
44. Vosko, S. H.; Wilk, L.; Nusair, M., Accurate spin-dependent electron liquid correlation energies for local spin density calculations: a critical analysis. *Can J Phys* **1980,** *58* (8), 1200-1211.
45. Stephens, P. J.; Devlin, F. J.; Chabalowski, C. F.; Frisch, M. J., Ab Initio Calculation of Vibrational Absorption and Circular Dichroism Spectra Using Density Functional Force Fields. *J Phys Chem* **1994,** *98* (45), 11623-11627.
46. Hehre, W. J.; Ditchfield, R.; Pople, J. A., Self—Consistent Molecular Orbital Methods. XII. Further Extensions of Gaussian—Type Basis Sets for Use in Molecular Orbital Studies of Organic Molecules. *J Chem Phys* **1972,** *56* (5), 2257-2261.
47. Hay, P. J.; Wadt, W. R., Ab initio effective core potentials for molecular calculations. Potentials for K to Au including the outermost core orbitals. *J Chem Phys* **1985,** *82* (1), 299-310.
48. Banks, J. L.; Beard, H. S.; Cao, Y.; Cho, A. E.; Damm, W.; Farid, R.; Felts, A. K.; Halgren, T. A.; Mainz, D. T.; Maple, J. R.; Murphy, R.; Philipp, D. M.; Repasky, M. P.; Zhang, L. Y.; Berne, B. J.; Friesner, R. A.; Gallicchio, E.; Levy, R. M., Integrated Modeling Program, Applied Chemical Theory (IMPACT). *J Comput Chem* **2005,** *26* (16), 1752-80.
49. Glendening, E. D..;Landis C. R.; Weinhold F, Natural bond orbital methods. *Wiley Int Rev Comput Mol Sci* **2012,** *2* (1), 1-42.
50. Armendáriz-Vidales, G.; Hernández-Muñoz, L. S.; González, F. J.; de Souza, A. A.; de Abreu, F. C.; Jardim, G. A. M.; da Silva, E. N.; Goulart, M. O. F.; Frontana, C., Nature of Electrogenerated Intermediates in Nitro-Substituted Nor-β-lapachones: The Structure of Radical Species during Successive Electron Transfer in Multiredox Centers. *J Org Chem* **2014,** *79* (11), 5201-5208.
51. Marenich, A. V.; Ho, J.; Coote, M. L.; Cramer, C. J.; Truhlar, D. G., Computational electrochemistry: prediction of liquid-phase reduction potentials. *Phys Chem Chem Phys* **2014,** *16* (29), 15068-106.
52. Isegawa, M.; Neese, F.; Pantazis, D. A., Ionization Energies and Aqueous Redox Potentials of Organic Molecules: Comparison of DFT, Correlated ab Initio Theory and Pair Natural Orbital Approaches. *J Chem Theory Comput* **2016,** *12* (5), 2272-2284.
53. Friesner, R. A., Modeling Metalloenzymes with Density Functional and Mixed Quantum Mechanical/Molecular Mechanical (QM/MM) Calculations: Progress and Challenges. *Encyclopedia of Inorganic Chemistry*, 2009.

54. Dynamics Studies of Metal Binding Proteins. *Biomolecules* **2014,** *4* (3), 616.
55. Khandelwal, A.; Lukacova, V.; Comez, D.; Kroll, D. M.; Raha, S.; Balaz, S., A Combination of Docking, QM/MM Methods, and MD Simulation for Binding Affinity Estimation of Metalloprotein Ligands. *J Med Chem* **2005,** *48* (17), 5437-5447.
56. Siegbahn, P. E. M.; Blomberg, M. R. A., Transition-Metal Systems in Biochemistry Studied by High-Accuracy Quantum Chemical Methods. *Chem Rev* **2000,** *100* (2), 421-438.
57. Lundberg, M.; Siegbahn P.E.M., Agreement between experiment and hybrid DFT calculations for O-H bond dissociation enthalpies in manganese complexes. *J Comput Chem* **2005,** *26* (7), 661-667.
58. Lovell, T.; Himo, F.; Han, W.-G.; Noodleman, L., Density functional methods applied to metalloenzymes. *Coord Chem Rev* **2003,** *238-239*, 211-232.
59. Murphy R. B.; Phillipp D. M.; Friesner R. A, A mixed quantum mechanics/molecular mechanics (QM/MM) method for large-scale modeling of chemistry in protein environments. *J Comput Chem* **2000,** *21* (16), 1442-1457.
60. Duffy, E. M.; Jorgensen, W. L., Prediction of Properties from Simulations: Free Energies of Solvation in Hexadecane, Octanol, and Water. *J Am Chem Soc* **2000,** *122* (12), 2878-2888.
61. 2018-2, S. R. *QikProp, Schrödinger,*, **2018.**
62. Schrödinger Release 2019-1: QikProp, S., LLC, New York, NY, **2019.**
63. Biotech, S. S. *Simca-P11.5*, **2013.**
64. Cecatiello, V., Pasqualato, S., Crystal Structures of Human Jmjd2C Catalytic Domain Bound to Inhibitors. ***2015.**, DOI: 10.2210/PDB5FJK/PDB*
65. Arpinelli, F.; Bamfi, F., The FDA guidance for industry on PROs: the point of view of a pharmaceutical company. *Health Qual Life Out* **2006,** *4* (1), 85.
67. Wring, S. A.; Shampine, L. J.; Serabjit-Singh, C. J.; Adkison, K. K.; Polli, J. W., Passive permeability and P-glycoprotein-mediated efflux differentiate central nervous system (CNS) and non-CNS marketed drugs. *J Pharmacol Exp Ther* **2002,** *303* (3), 1029-37.
67. Mueller, R. M.; North, M. A.; Yang, C.; Hati, S.; Bhattacharyya, S., Interplay of Flavin's Redox States and Protein Dynamics: An Insight from QM/MM Simulations of Dihydronicotinamide Riboside Quinone Oxidoreductase 2. J P*hys Chem B* **2011,** *115* (13), 3632-3641.
68. Latuasan, H. E.; Berends, W., On the origin of the toxicity of toxoflavin. *Biochim Biophys Acta* **1961,** *52*, 502-8.
69. Hall., L. H.; Orchard, B. J.; Tripathy, S. K., The structure and properties of flavins: Molecular orbital study based on totally optimized geometries. I. Molecular geometry investigations. *Int J Quantum Chem* **1987,** *31* (2), 195-216.
70. North, M. A.; Bhattacharyya, S.; Truhlar, D. G., Improved Density Functional Description of the Electrochemistry and Structure−Property Descriptors of Substituted Flavins. *J Phys Chem B* **2010,** *114* (46), 14907-14915.
71. Méndez-Hernández, D. D.; Tarakeshwar, P.; Gust, D.; Moore, T. A.; Moore, A. L.; Mujica, V., Simple and accurate correlation of experimental redox potentials and DFT-calculated HOMO/LUMO energies of polycyclic aromatic hydrocarbons. *J Mol Model* **2013,** *19* (7), 2845-2848.
72. Davis, A. P.; Fry, A. J., Experimental and computed absolute redox potentials of polycyclic aromatic hydrocarbons are highly linearly correlated over a wide range of structures and potentials. *J Phys Chem A* **2010,** *114* (46), 12299-304.

Conflicts of interest

There are no conflicts to declare.

Graphical Abstract

Rational design, synthesis and biological profiling of new KDM4C inhibitors

Leave this area blank for abstract info.

Vatroslav Letfus*, Dubravko Jelić, Ana Bokulić, Adriana Petrinić Grba, Sanja Koštrun
Fidelta Ltd., Prilaz baruna Filipovića 29, 10000 Zagreb, Croatia